Extended hygrothermal characterization of unstabilized rammed earth for modern construction

Alessia Emanuela Losini, Monika Woloszyn, Taini Chitimbo, Antoine Pelé-Peltier, Sahbi Ouertani, Romain Rémond, Maxime Doya, David Gaillard, Marie Sarah Force, J. Outin, et al.

Extended hygrothermal characterization of unstabilized rammed earth for modern construction

Alessia Emanuela Losini[1*], Monika Woloszyn[1], Taini Chitimbo[1], Antoine Pelé-Peltier[2], Sahbi Ouertani[3], Romain Rémond[3], Maxime Doya[4], David Gaillard[4], Marie Sarah Force[2], Jonathan Outin[1], Anne-Cecile Grillet[1], Noemie Prime[1]

[1] LOCIE, University Savoie Mont Blanc, Solar Academy, CNRS UMRS, 73370 Le bourget du lac, France;

[2]ENTPE, LTDS, UMR 5513 CNRS, ENTPE, Univ. Lyon, 2 rue Maurice Audin, 69120 Vaulx-en-Velin, France;

[3]Université de Lorraine, INRAE, LERMAB, 27 rue Philippe Séguin, 88051 Epinal, France;

[4] Tipee, Technological platform, 8 rue Isabelle Autissier, 17140 LAGORD, France;

*corresponding author: alessia.losini@univ-smb.fr

Keywords: rammed earth; hygrothermal properties; non-constant parameters; sorption isotherm; water vapor permeability; thermal conductivity; specific heat capacity.

Highlights:

- Extended hygrothermal characterization of unstabilized rammed earth.
- Low influence of density and grain size distribution on sorption isotherm.
- High influence of density on thermal conductivity and vapor resistance factor.
- Same linear dependency of thermal conductivity on moisture content for different soil compositions.
- Vapor transfer resistance factor for a large span of relative humidity.

Abbreviation: RE (rammed earth), DVS (dynamic vapor sorption), SSS (saturated salt solutions), MSDC (modulated differential scanning calorimetry), RH (relative humidity), GAB (Guggenheim-Anderson-de Boer), ADS (Asdorption), DES (Desorption).

Nomenclature:

Roman Symbols	Units	Description
A	m^2	area of the specimen
A_{-value}	$kg.m^{-2}.s^{-1/2}$	water absorption coefficient
b	m	width of the hidden edge
C_p	$J.kg^{-1}.K^{-1}$	specific heat capacity
$D_{\omega s}$	$m^2.s^{-1}$	liquid transport coefficient fro suction
$D_{\omega r}$	$m^2.s^{-1}$	liquid transport coefficient fro redistribution
d	mm	thickness of the specimen
d_a	mm	thickness of the air layer in the cup
e	$W.s^{0.5}.m^{-2}.K^{-1}$	thermal effusivity
J	$kg.m^{-2}.s^{-1}$	vapor flux densisty
m_0	kg	initial mass or dry mass
P_{sat}	Pa	saturation water vapor pressure
P_v	Pa	barometric water vapor pressure
R_v	$J.kg^{-1}.K^{-1}$	gas constant for water vapor
S	m	hydraulic diameter
T	°C	temperature in Celsius
ω	$kg.m^{-3}$	mass par volume water content
ω_f	$kg.m^{-3}$	free water saturation
Z	$m^2.s.Pa.kg^{-1}$	overall surface resistance to vapour transfer

Greek symbols	Units	Description
α	$m^2.s^{-1}$	thermal diffusivity
n	%	porosity
θ	K	temperature in Kelvin
λ	$W.m^{-1}.K^{-1}$	dry thermal conductivity
λ_w	$W.m^{-1}.K^{-1}$	moisture dependent thermal conductivity
$\boldsymbol{\beta}_{out}$	$kg.m^{-2}.s^{-1}.Pa^{-1}$	apparent mass exchange coefficient
δ	$kg.m^{-1}.s^{-1}.Pa^{-1}$	water vapour permeability of material
$\boldsymbol{\delta}_{air}$	$kg.m^{-1}.s^{-1}.Pa^{-1}$	water vapour permeability of still air
δ_r	$kg.m^{-1}.s^{-1}.Pa^{-1}$	actual permeability
μ	-	water vapour resistance factor
$\boldsymbol{\rho}_d$	$kg.m^{-3}$	dry density
ρ_l	$kg.m^{-3}$	liquid water density
φ	-	relative humidity
w	% ($kg.kg^{-1}$)	water content

Abstract

Although hygrothermal properties of rammed earth represent great potential for improving thermal comfort during hot summers, still little knowledge is available about this topic. The literature lacks complete sets of hygrothermal characteristics of rammed earth, although they are fundamental for heat and moisture transfer modeling necessary to predict earthen building performances. The present work reports the results

of a large collaboration between four academic laboratories in order to obtain an extended hygrothermal characterization of rammed earth, focusing on the material used in a modern construction in Lyon, France. The aim of the article is to provide for the same kind of soil an extend characterization on a large span of relative humidity to provide complete set of material properties for heat and moisture transfer simulation. The hygrothermal measurements cover adsorption and desorption isotherm, intermediate isotherm loop, specific heat capacity, dry thermal conductivity, moisture-dependent thermal conductivity and water vapor resistance factor for a large span of relative humidity. In addition, the capillary rise test was performed to estimate the liquid transport coefficient for suction and redistribution. The results show that variations in the density of the samples have a low impact on sorption isotherm, while they have a non-negligible impact on thermal conductivity and water vapor permeability. Surprisingly, variations in the grain size distribution do not produce a significant modification in the sorption isotherm, while hysteresis slightly reduces when bigger grains are added to the soil composition. Approximation of empirical model coefficients for the determination of moisture-dependent thermal conductivity is proposed for rammed earth materials.

1 Introduction and background

Building and construction sector has a very high environmental impact as it is responsible for about 30% of natural resource extraction and about the same amount of CO_2 emissions on global scale [1,2]. Moreover, it is estimated that about 48% of the global energy is consumed during building construction and lifetime, both as embodied and operational energy [3]. Therefore, an important effort is required to reduce the impact of the material used for building construction while maintaining good building performances and reducing energy consumption during the operative phase of the dwelling.

Earthen construction materials offer an opportunity to use sustainable materials with interesting hygrothermal properties and lower embodied energy [4]. Earthen houses host about 10% of the global population and 10% of UNESCO world heritage sites are earthen architectures [5,6]. Moreover, in France, around 7 and 10,000,000 tons per year of hazardous and non-hazardous waste from foundation excavation is produced [7]. The potential of using part of this large amount of soil is in line with the logic of circular economy and low carbon footprint [8]. Nowadays, the traditional technique is readopted and tested in

modern buildings, as in the case of *l'Orangerie*, a building in the Confluence district of Lyon, France (Figure 1) [9].

Among the different techniques of raw earth construction, rammed earth (RE) is one of the most used around the world. Soil with low moisture content is compacted layer by layer in formwork, composing a load-bearing wall. RE offers numerous advantages as a sustainable construction material: low embodied energy due to the local availability, low processing since no firing process is involved and it can be recycled at the end of life if no stabilizers are used [10]. RE presents elevated hygroscopic properties thanks to the presence of clay [11]. Water molecules are adsorbed and desorbed in the porous network and at the surface of fine particles, giving the material similar characteristics to phase change materials. The evaporation and condensation of water in the walls allow to release and store latent heat, postponing the heating and cooling of the walls [12,13]. For this reason, earthen houses are commonly considered particularly effective for passive regulation of indoor environment in hot climate conditions [14,15]. Moreover, RE walls present good passive regulation properties in the indoor environment, maintaining the relative humidity in a suitable range for human health [16,17].

However, a barrier to the use of earthen construction materials is the lack of knowledge of their hygrothermal properties and their responses to different climatic stresses [18]. The natural variability of the soil can modify the hygro-thermo-mechanical behavior of the earthen materials under real climatic conditions [19]. To facilitate the use of RE buildings it is essential to predict their energy performance, using dynamic thermal simulation and taking into account the combined (coupled) heat and moisture transfer in the wall and the non-constant hygrothermal properties [20–23]. One of the most used hygrothermal models was proposed by Kunzel and implemented in two engineering software: WUFI® (commercial software) and EnergyPlus™ (open source software) [24]. The complete set of hygrothermal properties requested by the model includes: dry density, porosity, sorption isotherm, water vapor resistance factor variations according to RH, specific heat capacity, dry thermal conductivity, thermal conductivity variations according to RH, liquid transport and redistribution coefficients [24]. Some studies start to provide an interesting dataset for other materials, such as straw-clay mixtures, reinforced earthen blocks, concrete and bio-stabilized rammed earth materials, nevertheless, a paper that reports an extended characterization of unstabilized RE material is still

missing, in particular regarding the variability of thermal conductivity and vapor permeability on a large span of relative humidity [25–27]

A literature review by Losini et al. [28] illustrated a large availability of literature reporting the mechanical properties of earthen materials, while the investigations of their hygrothermal properties are still limited. A detailed review by Giuffrida et al. [29] collects different measurements of hygrothermal properties of earthen materials and reports a lack of a complete set of hygrothermal characterization in the references about RE. In fact, the state of the art on this subject presents many articles focused on a single hygrothermal property, such as sorption isotherm or vapor permeability, but often the characterization does not cover all the material properties necessary for a combined heat and moisture transfer simulation [4,27,30–33]. Moreover, to provide a full data set for simulation, mixing data that belongs to different soils is not suitable, due to the high variability of soil compositions and techniques for sample preparations.

Figure 1: L'Orangerie, building in Lyon, dated 2019 made of pre-fabricated rammed earth.

The aim of this work is to present a comprehensive set of non-constant hygrothermal properties of unstabilized RE material to provide the necessary data for future studies on the RE energy performance using

combined heat and moisture transfer models. All tests were done on the same soil on a large span of relative humidity, providing detailed information of hygrothermal properties modification according to moisture content in the material. In addition, the investigated soil was used to erect a new RE building, providing interesting data for future studies on model validation and building scale (Figure 1). All the presented tests were conducted between 2019 and 2023 in four different laboratories, which will be cited for simplicity as laboratories A, B, C and D. The earth used is the same for all laboratories, although prepared differently and from two different batches (A and B).

2 Materials and methods

The material used was earth coming from St Quentin Fallavier, in the Auvergne-Rhone-Alpes region in Southeastern France. The soil was used for the construction of the already-mentioned l'Orangerie building (Figure 1).

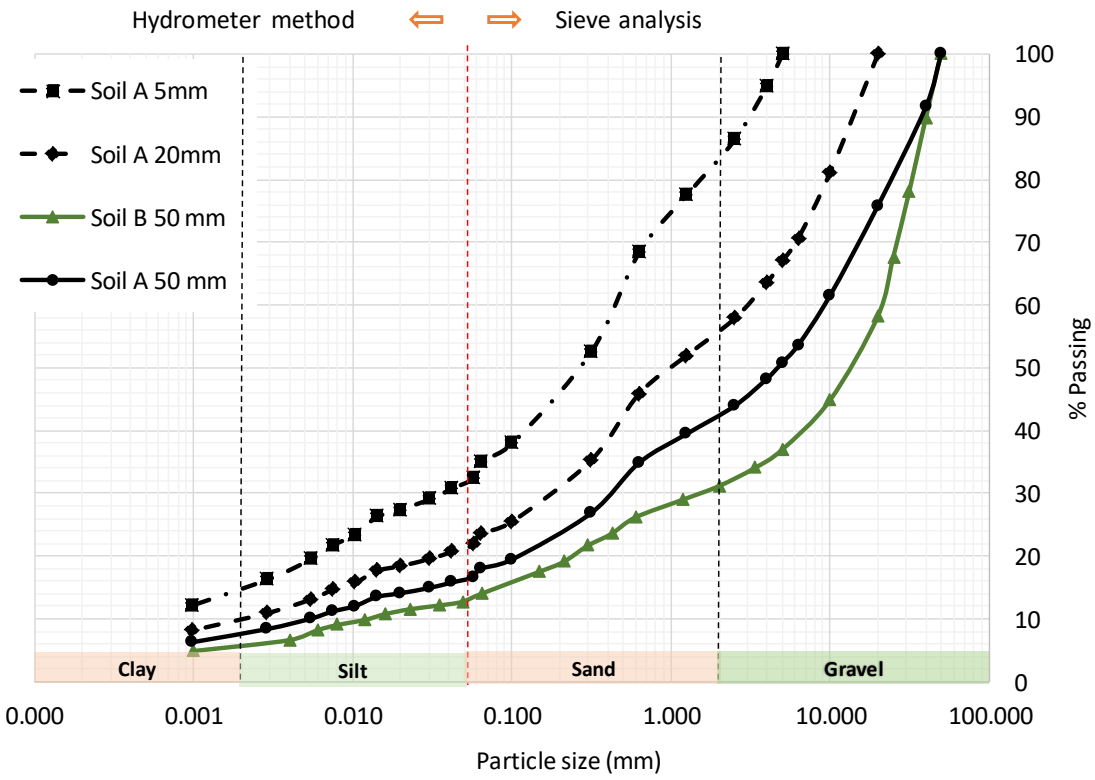

The particle size distribution curve was determined by using wet sieving and hydrometer analysis

Figure 2 Particle size distribution of two batches of the soil, tested respectively by laboratory A and B. Soil is sieved at 50, 20 and 5 mm.

according to French standards (NF P 94-057) in two laboratories (A and B). The grain size distribution curve

of laboratory B was published by Pelé-Peltier et al. [9] and the curve of laboratory A by Chitimbo et al. [34], both used in the experimental tests in different laboratories. Both curves are reported in Figure 2, showing a non-negligible difference in the two batches of soil sieved at 50 mm, with a maximum difference of 5% of passing. This may be due to the spatial variability of this natural material and shows the difficulty of working with non-standard construction material. The different samples used in the study were prepared with the grain size distribution rescaled at 5 mm and 20 mm as reported in Figure 2, adapting the material to samples at a laboratory scale. The Atterberg limits were determined on soil of laboratory A. The cone penetrometer results were verified to be in accordance with Casagrande method and present a liquid limit at 30% of water content, a plastic limit at 19.1% and a plastic index at 10.9% [34]. This value shows a low plasticity of fine particules. The methylene blue value of earth was measured at 1.35 g/100 g, which indicate low swelling activity in accordance with the low index of activity, around 3.5 [34].

2.1 Samples preparation

Different samples were prepared with the aim of testing the material used for the building site in Lyon. The RE blocks used on-site present an average dry density of 1930 $kg.m^{-3}$ and were made using the soil sieved at 50 mm and a manufacturing water content between 8 and 9.6%. To prepare smaller samples for different tests, the original soil was sieved at three different grain size diameters: 50 mm, 20 mm and 5 mm. Different compaction methods were adopted, in order to obtain a dry density near to the building one. Table 1 lists all the samples prepared in the different laboratories andin which laboratory they are tested. Each batch of samples is manufactured and tested in the same conditions (testing laboratory gives the letter name of the batch). Other important information as the technique of preparation, sample dimensions, number of samples prepared, dry density and water content used for sample preparation are also reported. More details about the preparation of samples A1 and A4 can be found respectively in the studies by Chauhan et al. [19] and Chitimbo et al. [34].

Table 1 List of samples and technique of preparation, dimensions, dry density and initial mass water content (w).

Prepared by laboratory	Batch name	Preparation	Maximum grain size (mm)	Samples dimension (cm)	Numb.	Dry density ($kg.m^{-3}$)	W (%)
A	A1	Double compression	5	Ø=5, h=1.5	4	1855	9.6
B	A2	Static compression	5	Ø=7, h=2	20	2022 ± 4	-
B	D1	Static compression	5	Ø=7, h=1.3	20	1985 ± 24	-

B	A3	Static compression	5	Ø=10, h=3	20	1943 ± 12	-
B	B1	Dynamic compaction	5	Ø=10.1, h=2.2	2	1930 ± 10	8.5
B	B2	Dynamic compaction	5	Ø=10.1, h=2.1	2	1660 ± 20	8
B	B3	Dynamic compaction	5	Ø=10.1, h=4.15	2	1660 ± 20	8
B	B4	Dynamic compaction	5	Ø=10.1, h=6.4	2	1660 ± 20	8
A	A4	Dynamic compaction	20	15 x 15 x 45	2	1883 ± 13	9.6
B	B5	Dynamic compaction	50	Ø=15.1, h=11.7	4	1940 ± 0.01	8.3

2.1 Experimental organization

The experimental tests were done in 4 different laboratories on different types of samples, as reported in Figure 3 and Table 2. Table 2 reports the laboratory which executed the test, the applied experimental method, the number of tested samples, the repetitions of the test on each sample, and the dimensions of the sample. Sorption isotherms were tested by dynamic vapor sorption (DVS) and by saturated salt solutions (SSS). Thermal conductivity was determinated by C-Therm and Hot Disk apparatus in two different laboratories. Moreover, the thermal conductivity variations according to moisture content were tested at 7 different levels of RH%. Water vapor permeability was tested by wet and dry cup in two laboratories. To complete the characterization of hygrothermal parameters, the heat capacity was

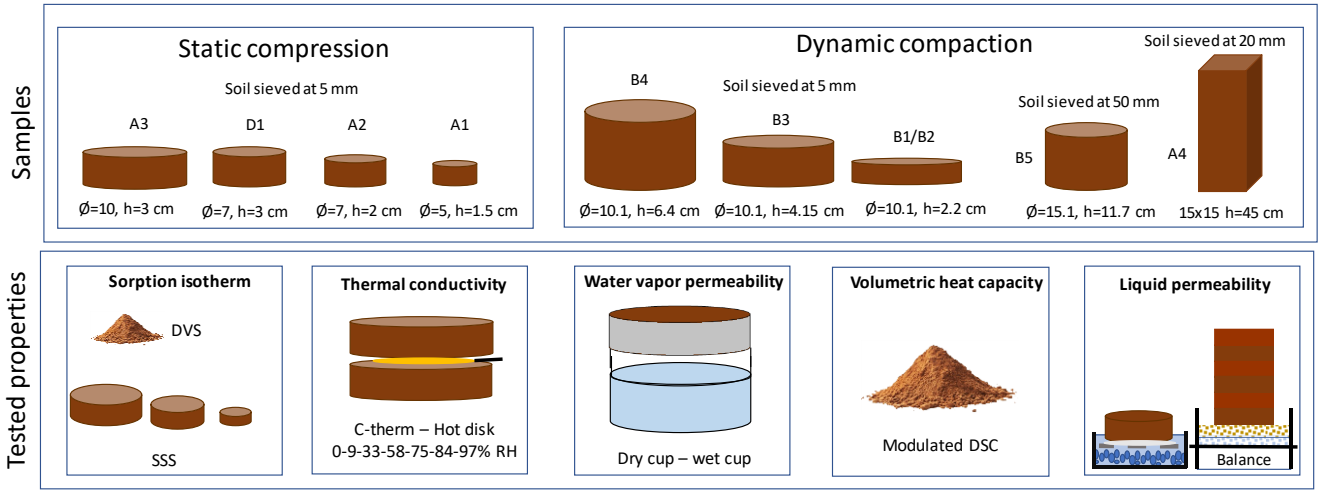

Figure 3 Synthetic view of performed characterisations.

determinated by modulated differential scanning calorimeter (MDSC). Capillary rise test was also performed to evaluate the liquid transfer coefficient of the soil.

*Table 2 List of tested properties. *Results from sample A1 were already published by Chitimbo et al.* [34]*, here reported for comparison.*

properties	Laboratory of test	Batch samples	Experimental method	# samples	Repetition/ sample	Samples dimension
Grain size distribution	A/B	soil	Sedimentation/sieving	-	-	-
Sorption isotherms	A*	A1	Saturated salt solutions	4	-	Ø=5, h=1.5 cm
	A	A2	Saturated salt solutions	4	-	Ø=7, h=2 cm
	A	A3	Saturated salt solutions	4	-	Ø=10, h=3 cm

	A	A4.1	Saturated salt solutions	3	-	Blocks of 500 g
	C	soil	Dynamic vapor sorption	1	1	50 mg
	B	soil	Dynamic vapor sorption	1	-	660 mg
Thermal Conductivity λ at 58% RH	A/C	A3	Hot Disk	6	4	Ø=10, h=3 cm
	A	A3	C-Therm	2	4	Ø=10, h=3 cm
λ at 0-9-33-58-75-84-95%% RH	A	A2	Hot Disk	4	4	Ø=7, h=2 cm
	A	A3	Hot Disk	4	4	Ø=10, h=3 cm
Heat capacity	A	soil	Modulated DSC	3	1	20 mg
Vapor permeability	D	D1	Wet -dry cup	6	2	Ø=7, h=1.3 cm
	B	B1,2,3,4	Wet cup	8	-	Ø=10.1, h=2.1-6.3 cm
Liquid transport coefficient	A	A4	Capillary rise	2	-	15 x 15 x 45 cm3
	B	B5	Capillary rise	4	-	Ø=15.1, h=11.7 cm

2.2 Sorption isotherm

A material with an "open" porosity, such as earth, has the capacity to exchange humidity with the ambient air: adsorb or release humidity by fixing water molecules on pores surface, leading to an apparent mass gain or loss of the earthen sample. When the material is in equilibrium with the surrounding RH, its weight is stabilized and it is possible to estimate the mass of the water adsorbed for a given RH% at a constant temperature, determining the sorption and desorption isotherm. The moisture adsorption is calculated in reference to the initial dry conditions with the following formula:

$$w = \frac{m - m_o}{m_o} \quad (1)$$

where m_0 is the dry mass and m is the mass measured at equilibrium at different RH levels.

The sorption isotherm was measured with the dynamic vapor sorption (DVS) technique by two laboratories (B and C) [35]. The saturated salt solution (SSS) technique was used in A laboratory on 3 different types of samples (A1,2,3). Some blocks extracted from A4 samples were also tested, and are reported as A4.1 batch. GAB (Guggenheim-Anderson-de Boer, [36,37]) model (eq. (2)), has been used with least square method to interpolate all the curves, as reported in the following equation:

$$w = \frac{C_1 \cdot C_2 \cdot \varphi}{(1 - C_2 \cdot \varphi) \cdot (1 - C_2 \cdot \varphi + C_1 \cdot C_2 \cdot \varphi)} \cdot w_m \quad (2)$$

Where C_1 , C_2 and w_m are fitting parameters of the model and φ the relative humidity.

2.2.1 Dynamic vapor sorption

Dynamic Vapor Sorption (DVS) method consists in measuring moisture uptake and loss by flowing air at a specified relative humidity through a small sample (a few milligrams) of soil suspended from the weighing mechanism of a microbalance. The variations of the relative humidity are automatically performed by the instrument when the target condition of mass stability is reached. The reference dry mass used by DVS for the calculation of the water content is obtained by drying in dry air (0.6 ± 0.1% RH) at 23°C. The transition to the next condition is made according to the chosen equilibrium criterion on the mass variation ($dm.m^{-1}$), fixed at 0.0005% per minute. The stability duration of the $dm.m^{-1}$ criterion was fixed to 10 min.

2.2.2 Saturated salt solutions

The adsorption and desorption isotherms were measured following the recommendation of the international standard ISO 12571:2013(E) [38]. The samples were dried in an oven at 105°C until equilibrium and then placed in desiccators to lower their temperature and to measure their dry mass (m_0). The samples were wrapped in transpiring non-hygroscopic fabric that enables the transfer of water vapor while preserving the integrity of the samples, avoiding the risk of fragment loss during weighing. RH% levels were generated in air-locked containers by different saturated salt solutions. Different salts were used (i.e., KOH, CH_3CO_2K, $MgCl_2$, NaBr, NaC, KCl, and K_2SO_4) to produce 7 stable levels of RH (9%, 22%, 33%, 58%, 75%, 84%, and 97%) [38,39]. Moreover, humidity and temperature conditions were monitored for additional verification by hygrothermal sensors (precision ±3% RH and ± 0.5°C) placed inside the containers. A balance with a precision of ±1 mg was used for measuring the mass of the samples (Ohaus Corporation). The mass of the samples was recorded every 24 h, until reaching equilibrium (mass variation lower than 0.01% for two consecutive days). This criterion was increased from 0.1% (standard recommendation) to 0.01% due to the high density of RE compared to the usual hygroscopic materials considered by the reference standard ISO [38].

Comparability of the different techniques of measurement

Some differences in the execution of the test are worth to be summarized, as reported in Table 3, to assess the comparability of the different techniques of measurement. No correction was applied to the different temperatures of measurement (23-25°C) since the difference of only two degrees is considered

negligible. However, some corrections are here proposed to allow the comparison of the curves dried at 23 or 105°C.

Table 3 Methods for sorption isotherm measurements in the different laboratories.

Temperature	Laboratory	Technique	Sieved (mm)	Samples dimension	Drying temperature (°C)	n. samples	Batch	Density (kg.m^{-3})
23 ± 2°C	A	SSS	5	Ø=5, h=1.5 cm	105	4	A1	1855
	A	SSS	5	Ø=7, h=2 cm	105	4	A2	2022 ± 4
	A	SSS	5	Ø=10, h=3 cm	105	4	A3	1943 ± 12
	A	SSS	20	Blocks of 500 g	105	3	A4.1	1883 ± 13
	C	DVS	5	50 mg	23	1	-	-
	B	DVS	1	660 mg	23	1	-	-

The reference dry mass used for the soil characterization tests is generally obtained by drying at 105°C for SSS. The difference in the drying temperature may result in a translation of the DVS curve towards higher values of water content. Fabbri et al. [35] proposed a correction for comparing sorption isotherms obtained by different methods, which relies on the residual moisture content w_0 between the mass dried at 23°C, named $m_{\_23}$, and the mass dried at 105°C, named $m_{\_105}$. The equation here proposed was verified and corrected with respect to the one published by Fabbri et al. [35], which presented a problem in the order of numerator and denominator.

It is, therefore, necessary to modify the water content measured by the DVS in order to take into account this difference in drying mode for the estimation of m_0, by applying the following equation:

$$w_c = (1 + w_0) \cdot w_{DVS} + w_0 = \frac{m_{\_23}}{m_{\_105}} \cdot (w_{DVS} + 1) - 1 \quad (3)$$

where w_c is the corrected moisture content equivalent of samples dried at 105°C, w_{DVS} is the measured moisture content by DVS at 23°C, and w_0 was determinated here as equal to 0.2% (laboratory B).

2.3 Water vapor permeability

The water vapor permeability δ (kg.m^{-1}.s^{-1}.Pa^{-1}) was determined with a procedure inspired by the international standard: EN ISO 12572 [40]. Vapor permeability tests impose two different relative humidity values at the two sides of a sample, comprising the vapor flow direction by sealing the lateral sides. The

samples are generally sealed on a cup containing saturated salt solution to create different RH%. The water vapor can flow through the specimen due to the difference in the partial vapor pressure outside and inside the cup. Two types of tests can be performed, the "wet cup" test and the "dry cup" test. The dry cup test sets a very low relative humidity inside the cup and higher ambient humidity. The vapor flow is thus directed toward the interior of the cup. In the case of the "wet cup" test, the vapor flow is inverted, and the higher RH% is in the cup, while the lower RH% is in the outdoor environment.

In the case of a wet cup test at high relative humidity, the capillary condensation process starts to fill pores with water, increasing the transport of liquid water while the vapor transport is reduced [40]. Therefore, the measured water vapor resistance factor μ does not only represent the vapor transport within the material but also the liquid water transport.

Once a steady flow is reached, by measuring the mass change of the device over time, the vapor permeability can be determined by the following procedure starting with the mass flow:

$$G_{line} = \frac{\mathrm{m}_1 - \mathrm{m}_2}{\mathrm{t}_1 - \mathrm{t}_2} \quad (4)$$

where m_1 (kg) is the mass at time t_1, and m_2 is the mass at time t_2, with t_1 and t_2 measurement time (s). Excluding the first part of the nonlinear phase of the test, a regression line is calculated between the mass increment and time of measurement, giving the slope G_{line} (kg.s^{-1}).

Water vapor permeability δ (kg.m^{-1}.s^{-1}.Pa^{-1}) is then estimated using the following formula:

$$\delta = \frac{d}{\frac{\mathrm{A} \cdot \Delta Pv}{G_{line}}} \quad (5)$$

where A is the sample area (m^2), d (m) is the thickness of the sample and ΔPv (Pa) is the difference in water vapor pressure between the two faces of the specimen.

The water vapor resistance factor, representing the ratio between the vapor permeability of the material to the one of still air, is generally expressed as:

$$\mu = \frac{\delta_{air}}{\delta_{material}} \quad (6)$$

The water vapor permeability of air δ_{air} (kg.m^{-1}.s^{-1}.Pa^{-1}) can be calculated with the formula below [40]:

$$\delta_{air} = \frac{0.086 \cdot P_0}{R_V \, \theta \, P} \left[\frac{\theta}{273}\right]^{1.81} \quad (7)$$

Where P_0 (101325 Pa) is the standard atmospheric pressure, P (Pa) and θ (K) are the barometric pressure and the temperature measured at experimental conditions, and R_v (462 J.kg^{-1}.k^{-1}) is the gas constant for water vapor.

Test procedure in laboratory B

The samples were hermetically sealed, using aluminum tape, to plastic cups containing a saturated salt solution set at 95% using KNO_3. The cups were then placed in a climatic chamber with 80% RH. These conditions allow us to investigate the vapor permeability in the capillary domain since the inflection point of the sorption curve is near 75% RH.

The test lasted until a good correlation in the measurements of G_{line} was obtained (40 days). For the 4 samples 2 cm and 4 cm thick, at least 11 points were retained with an R^2 higher than 0.995. In the case of the samples 6 cm thick, only five points reached the steady state with a correlation coefficient higher than R^2>0.98.

Masked edge effect corrections

In case the edge of the specimen overlaps the edge of the cup, a 'masked edge' can be created, and the water vapor permeability can be overestimated. This effect must be accounted for in the result by applying a correction factor using the following formula (Annex F of 2016 version of ISO 12572) [40] :

$$\frac{J_{vme}}{J_v} = 1 + \frac{4 \cdot d}{\pi \cdot S} ln\left(\frac{2}{1+exp\left(-\frac{2 \cdot \pi \cdot b}{d}\right)}\right) \quad (8)$$

Where: J_v (kg.m^{-2}.s^{-1}) is the vapor flux when correcting for the masked edge effect, d (m) is the thickness of the specimen; b (m) is the width of the hidden edge, S (m) is the hydraulic diameter (four times the test area divided by the perimeter) and J_{vme} (kg.m^{-2}.s^{-1}) is the vapor flux density measured in the presence of a masked edge, calculated by :

$$J_{vme} = \frac{G_{line}}{A} \quad (9)$$

Where A (m²) is the exchange surface of the sample (arithmetic average between the exposed surfaces inside and outside the device).

Surface convection effect corrections (laboratory B)

Different studies showed that it is important to take into account the surface convection effect which tends to overestimate the water vapor resistance factor of earthen samples [41,42]. It has been shown that the overall surface resistance (Z, $m^2.s.Pa.kg^{-1}$) can be determined using specimens of different thicknesses and plotting the apparent permeabilities versus thickness. The overall surface resistance can be estimated when the thickness of the material tends to zero [41,43,44] following equation (10):

$$\lim_{d\to 0}\left(\frac{d}{\delta}=\frac{d}{\delta_r}+Z\right)=Z \quad (10)$$

Where δ is the permeability corrected for the masked edge effect, d is the thickness of the sample, and δ_r ($kg.m^{-1}.s^{-1}.Pa^{-1}$) is the actual permeability.

$$\delta_r=\frac{1}{\frac{1}{\delta}-\frac{Z}{d}} \quad (11)$$

To determine the coefficient Z, equation (11) was used to plot the thickness/permeability ratio as a function of the thickness. The coefficient Z corresponds to the intercept of the line, and represents the global surface resistance during the cup test (below and above the specimen), as expressed in equation (12):

$$Z=Z_{int}+Z_{ext}=\frac{d_a}{\delta_a}+\frac{1}{\beta_{out}} \quad (12)$$

Where Z_{int} corresponds to the surface resistance inside the cup due to vapor diffusion through the air layer and Z_{ext} is the surface resistance above the cup, due to mass convection. β_{out}($kg.m^{-2}.s^{-1}.Pa^{-1}$) is the apparent mass exchange coefficient of surface water vapor transfer on the external side of the sample [41,45]. In case of a ventilation system in the climatic chamber, the β_{out} can be neglected and the correction of the internal air layer should be sufficient

Test methodology in Laboratory D

The water vapor permeability was determined using automated equipment allowing the gravimetric measurements of 6 samples per campaign (Gravitest 6400 from GINTRONIC). The equipment automatically performs periodic weightings (electronic balance accuracy 0.001 g) of the assembly to determine the steady-state water vapor transmission rate.

To adapt the cup of the automated equipment (79.8 mm) to the sample dimensions (70 mm), samples were prepared separately in PVC templates serving as a mold to pour melted microcrystalline wax around. A piece of sulfurized paper was used as a bottom. Once dried, the assembly was sealed on the cups with a second layer of wax. This procedure also allowed eliminating the masked edge effect. The surface open to air was accurately measured (about 38 cm^2) and the thickness (13.8 ± 5 mm) with a micrometer comparator. The samples were preconditioned at 50% and 23°C RH before starting the experiment. The wax seal had an equivalent air layer thickness (Sd-value) greater than 70 m. The cups were filled with different salt solutions (LiCl, $Mg(NO_3)^2$, KCl, $CaCl_2$) to impose a different RH (11%, 50%, 85%). The cups were then placed at 23°C in a climatic chamber able to simulate different RH as detailed in Table 4. A total of 6 samples were tested, and each sample was subjected to 4 different humidities applied in dry-cup and wet-cup. A detailed plan of the test is reported in Table 4 in the results section.

Correction for resistance of air layers - laboratory D

The air velocity inside the climatic chamber was set at 0.25 $m.s^{-1}$ to reduce the resistance of the air layer above the test cup. Therefore, only the diffusion resistance of the air layer (d_a/δ_{air}) inside the cup between the internal face of the samples and salt solution was considered [41,43,45] as follows:

$$\delta = \frac{d}{\frac{S \cdot \Delta Pv}{G_{line}} - \frac{d_a}{\delta_{air}}} \quad (13)$$

Where d is the thinkness of the specimen and d_a is the thickness of the air layer in the cup between the sample and the salt solution.

2.4 Specific heat capacity (laboratory A)

MDSC (Modulated Differential Scanning Calorimeter) method was used, normalized to ASTM E1952 and E2716 with sapphire as the reference standard [46]. The DSC-25 from TA Instrument® allowed obtaining measurements in a range from 10 to 50°C with a heating rate of 2 $K.min^{-1}$, an oscillation period of 120 seconds and an amplitude of 0.64°C. The measurements were performed on three samples of about 20 mg.

The specific heat capacity c_p ($J.kg^{-1}.K^{-1}$) of the material was also calculated from the conductivity and effusivity measurements obtained with the C-Therm thanks to the following relation :

$$c_p = \frac{e^2}{\rho \cdot \lambda} \quad (14)$$

Where e is effusivity ($W.s^{0.5}.m^{-2}.K^{-1}$), λ thermal conductivity ($W.m^{-1}.K^{-1}$) and ρ_d is the dry density ($kg.m^{-3}$).

2.5 Thermal conductivity, thermal diffusivity and effusivity

C-Therm - laboratory A

The thermal conductivity of the materials was measured using a device from the company C- Therm based on the modified transient plane source technique. It uses a unilateral sensor and therefore requires the use of a single sample, unlike the conventional methods, and a contact agent (grease) in case of samples with rough surfaces such as RE. Due to the use of the contact agent, the samples can be used only for a limited number of measurements. Effusivity and thermal conductivity were measured directly and quickly at room temperature, providing insight into the thermal characteristics of the material. The four samples used were conditioned to 58% RH before the measurements. At least 6 measurements were done in a different location on the surface of each sample. The thermal diffusivity and heat capacity were then calculated from the thermal conductivity, specific heat capacity and density of the material.

Hot Disk apparatus – laboratory A, C

Conductivity measurements were performed with a Hot Disk apparatus (Transient Plane Source method) from ThermConcept (TPS 2500S model Laboratory A, TPS 1500 laboratory C). A probe with a double spiral in nickel with Kapton insulation was used for the measurement, model 5501 F1 with a radius of 6.403 mm. The thermal conductivity measurements were carried out according to the manufacturer's recommendations, i.e. (i) the total characteristic time in the range of 0.33 and 1, (ii) the total temperature increase of the sample between 2 and 5 °C, (iii) the standard deviation on the temperature maintained lower than 10^{-4} and 10^{-5} K. Thermal conductivity and diffusivity were directly measured, by placing the sensor between two samples, injecting a constant electrical power in the sensor, and detecting temperature variations in the samples. Since no contact agent is required, the samples can be used for several measurements. The analysis of the increment of the temperature was performed with the Hot Disk 'Thermal Analyzer' software using the isotropic module.

The advantage of rapid dynamic measurements is the reduction of time necessary for one measurement (of 1-2 min), therefore, it is possible to maintain the conditioning of the specimens at a specific temperature and relative humidity. To verify the reproducibility of the test, the samples were conditioned directly at 58% RH and measured in both laboratories. In laboratory A, the samples were also measured at different steps of the sorption and desorption isotherm curve (0-22-33-58-75-84-98%) for two different samples A2 and A3.

To test thermal properties of dry material, the samples were dried in an oven at 105°C until they reached equilibrium in weight (mass variations less than 0.01 % for 24 hours), then stored in boxes with silica gel at about 23°C. For measuring other levels of RH%, boxes with saturated salt solutions were used.

Thermal diffusivity

The thermal diffusivity (α, $m^2.s^{-1}$) was directly measured by Hot Disk apparatus. In the case of C-Therm, the diffusivity was determined by calculation using the following equation:

$$\alpha = \frac{\lambda}{\rho \cdot c_p} \quad (15)$$

Given the density of the material and its specific heat capacity.

Thermal effusivity

The thermal effusivity (e, $W.s^{0.5}.m^{-2}.K^{-1}$) was directly measured by C-Therm. In the case of Hot Disk measurements, the thermal diffusivity was calculated using the following equation:

$$e = \sqrt{\lambda \cdot \rho \cdot c_p} \quad (16)$$

2.6 Liquid transport coefficient and capillary absorption test

Liquid transport coefficient D_ω ($m^2.s^{-1}$) characterizes the ability of a material to absorb by capillarity and transport liquid water through its pore network. In the case of earthen materials, it is difficult to determine experimentally the liquid transport coefficient of unsaturated porous materials, as outlined by Soudani et al. [47]. The most widely used method is an indirect determination proposed by Kunzel [24]. Based

on capillary rise tests, the liquid transport coefficient is determined from the water absorption coefficient $A_{\_value}$ ($kg.m^{-2}.s^{-1/2}$), following this relation:

$$D_{\omega s}(\omega) = 3.8 \cdot \left(\frac{A_{\_Value}}{\omega_f}\right)^2 \cdot 1000^{\left(\frac{\omega}{\omega_f}-1\right)} \quad (17)$$

Where $D_{\omega s}$ ($m^2.s^{-1}$) is the capillary transport coefficient also called *liquid transport coefficient for suction*, depending on the mass par volume water content ω ($kg.m^{-3}$) and ω_f ($kg.m^{-3}$) free water saturation. The liquid transport coefficient for redistribution $D_{\omega r}$ ($m^2.s^{-1}$) can be calculated as one decimal power below the liquid transport coefficient for suction [24].

The capillary absorption test allows measuring the $A_{\_value}$ and ω_f. The initial condition used for the material characterization tests is generally obtained by drying at 105°C or by calculation using the sorption curve, giving reference dry mass, m_0 (kg). Samples are then partially immersed in the experimental setup for the capillary absorption test with a constant immersion level. By periodical weighting, the mass of liquid water absorbed over time is determined. During tests, 2 phases may occur. The first transitory one is the absorption process by capillary phenomenon. The second phase is the stabilization phase when the material reaches saturation. The water absorption coefficient, $A_{\_value}$, is determined by measuring the cumulative absorbed mass of water per unit area of the inflow surface, m_c ($kg.m^{-2}$) as follows:

$$m_c = \frac{m_i - m_0}{S} \quad (18)$$

where S is the sample area (m^2), m_0 is the dry mass, m_i (kg) is the mass at time t_i. During the absorption phase of the test, the regression line is calculated between the cumulative absorbed mass and the square root of the elapsed time, giving the $A_{\_value}$ ($kg.m^{-2}.s^{-1/2}$).

$$A_{value} = \frac{m_c}{\sqrt{t_i}} \quad (19)$$

Free water saturation

The free water saturation ω_f is obtained once the sample is saturated at the end of the test, by the following formula:

$$\omega_f = \frac{m_{sat} - m_0}{m_0} \cdot \rho_d \quad (20)$$

Where, m_{sat} (kg) is the sample mass when saturation is reached, and ρ_d (kg.m^{-3}) is the dry density. This latter parameter can be also estimated through theoretical definition, following these formulas by Fabbri et al. and Al Haffar [44,48]:

$$\omega_f = \frac{\rho_l}{\rho_d} \cdot n = \rho_l . \left(\frac{1}{\rho_d} - \frac{1}{\rho_s}\right) \quad (21)$$

Where ρ_l (kg.m^{-3}) is the liquid water density, ρ_s (kg.m^{-3}) the grain density and n the porosity.

Experimental setup – laboratory B

The water absorption coefficient A_{value} was measured following the international standard EN ISO 15148 [49]. The lateral sides of the samples were sealed, to impose unidirectional moisture ingress on the bottom side and the top surface was left open. The experimental set-up combines the use of filter paper to avoid dissolution of the soil in water, and a basket, recovering material from specimen disaggregation as illustrated in Figure 4 [12,48]. This element did not participate in the absorption phenomena, and its mass was taken into account for the calculations of the mass of absorbed water (Figure 4). The sample was immersed in 3 mm of water on a bed of gravel. The ambient temperature was set at 17.5°C and 50±5% RH.

Experimental setup – laboratory A

The experimental setup is inspired by the British Standard BS 3921 and Indeku et al. [31,50], it is described more in detail by Chitimbo et al. [51]. Only two out of four of the lateral sides of the samples were confined. The experimental device used fine sand as medium support, avoiding direct contact with the samples with water, as reported in Figure 4. Two plastic containers were connected by a siphon pipe maintaining the water level constant. The first container, hosting the sample and fine sand, was placed on a high-precision balance for continuous mass measurement. In the second container, the water level was maintained constant by a water reservoir system. 2 cm of sand was maintained out of the water level, equal to imposed the value of suction of 0.2 kPa [51], already in the saturated zone of the sorption curve. The test was performed at an ambient temperature of 21±2°C and RH of around 50±5%.

Although the two methods implemented by laboratory A and B are quite different, the boundary conditions at the base between the two test methods are similar since both are in the saturated state, with low suction values.

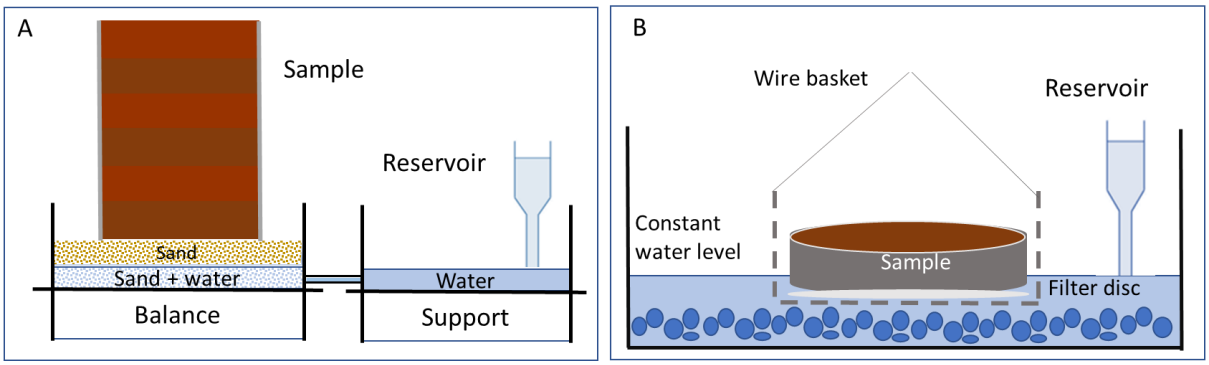

Figure 4: Diagram of the setup for the liquid permeability test used by laboratory A on the right and laboratory B on the left.

3 Results and discussion

3.1 Sorption isotherm

Sorption isotherm curves were determined by DVS in laboratory B, and by SSS in laboratory A on 4 different types of samples, as reported in Table 3, with the error bars for SSS tests. Considering the differences in the execution of the tests, the curves determined by the two methods will be first analyzed separately, then cross-compared. Table 3 reports a summary of the different tests. For all the curves, their shape suggests a similarity with the type II isotherm described by IUPAC, typical of clayish materials [52]. All the curves reach a maximal water retention of around 3-4% of water content for about 98% RH, in accordance with literature values (between 2.5-5% of water content variation) [11,48].

Dynamic vapor sorption – laboratory B and C

Figure 5 reports the sorption isotherms measured by DVS in laboratories B and C. Curve B was measured on about 660 mg of soil sieved at 1 mm, while curve C was on about 50 mg of soil from a bigger sample with a granulometry of up to 5 mm. Despite the difference in the two tests, Figure 5 shows how the two curves present a surprising correspondence in the shape and measured values. Curve C can be considered as an intermediate loop at lower RH (85%), which shows as expected a lower hysteresis.

Conversely, the equilibrium water content at 85% for curve C is higher than the curve B adsorption branch and corresponds better to the points of the desorption branch in curve B.

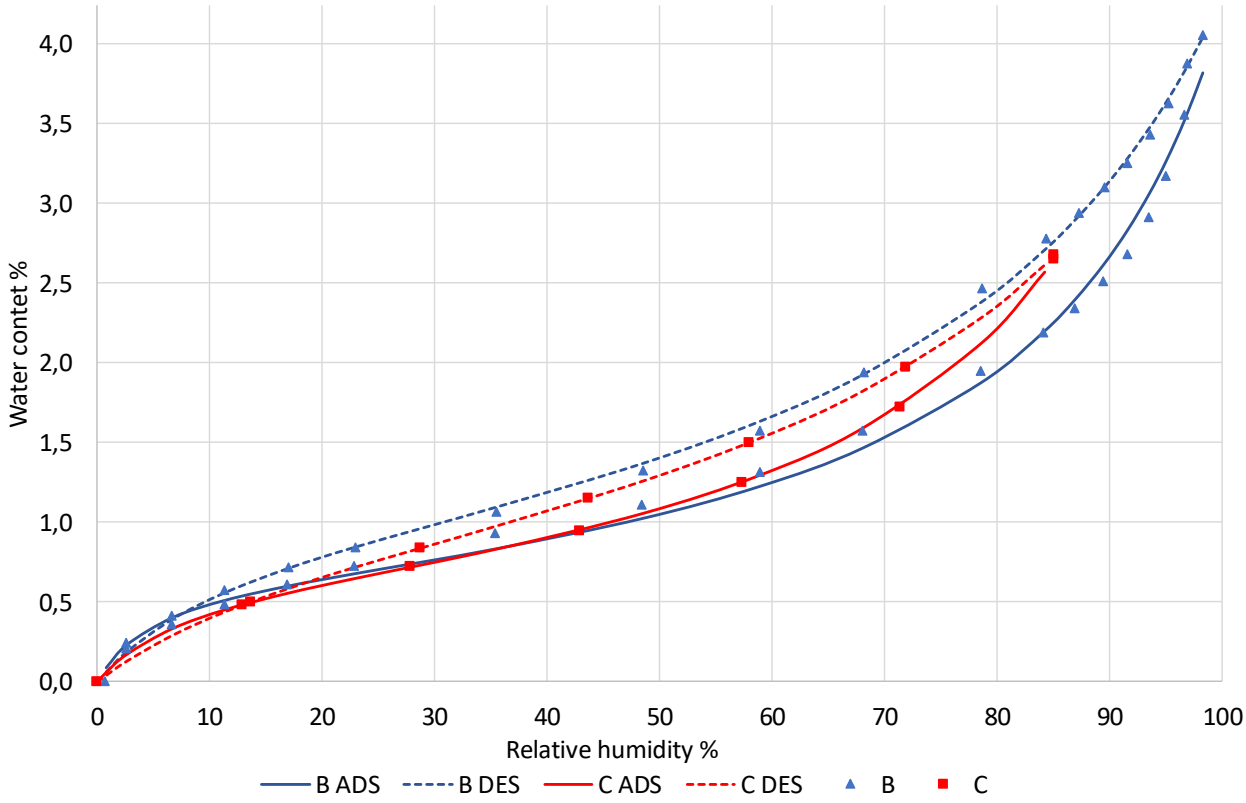

Figure 5 Sorption isotherm by DVS at 23±2°C. Measured points are reported with the interpolated curve using GAB model. 'DES' stands for 'Desorption', 'ADS' stands for 'Adsorption'.

Saturated salt solutions – laboratory A

Figure 6 reports the curves determined by SSS on four different types of samples (A1, A2, A3 and A4.1). All the samples have the same grain size distribution (sieved at 5 mm) except for A4.1 (sieved at 20 mm). Four samples were used to determine the moisture adsorption/desorption curve and the average of their measurements was used to define the final curve. The standard deviation of the measurement of the four samples was always verified to be lower than 5% for low levels of RH (less than 75%). The standard deviation increased for high levels of RH% up to 11%, showing the difficulty to use SSS for levels of RH which are near 100%.

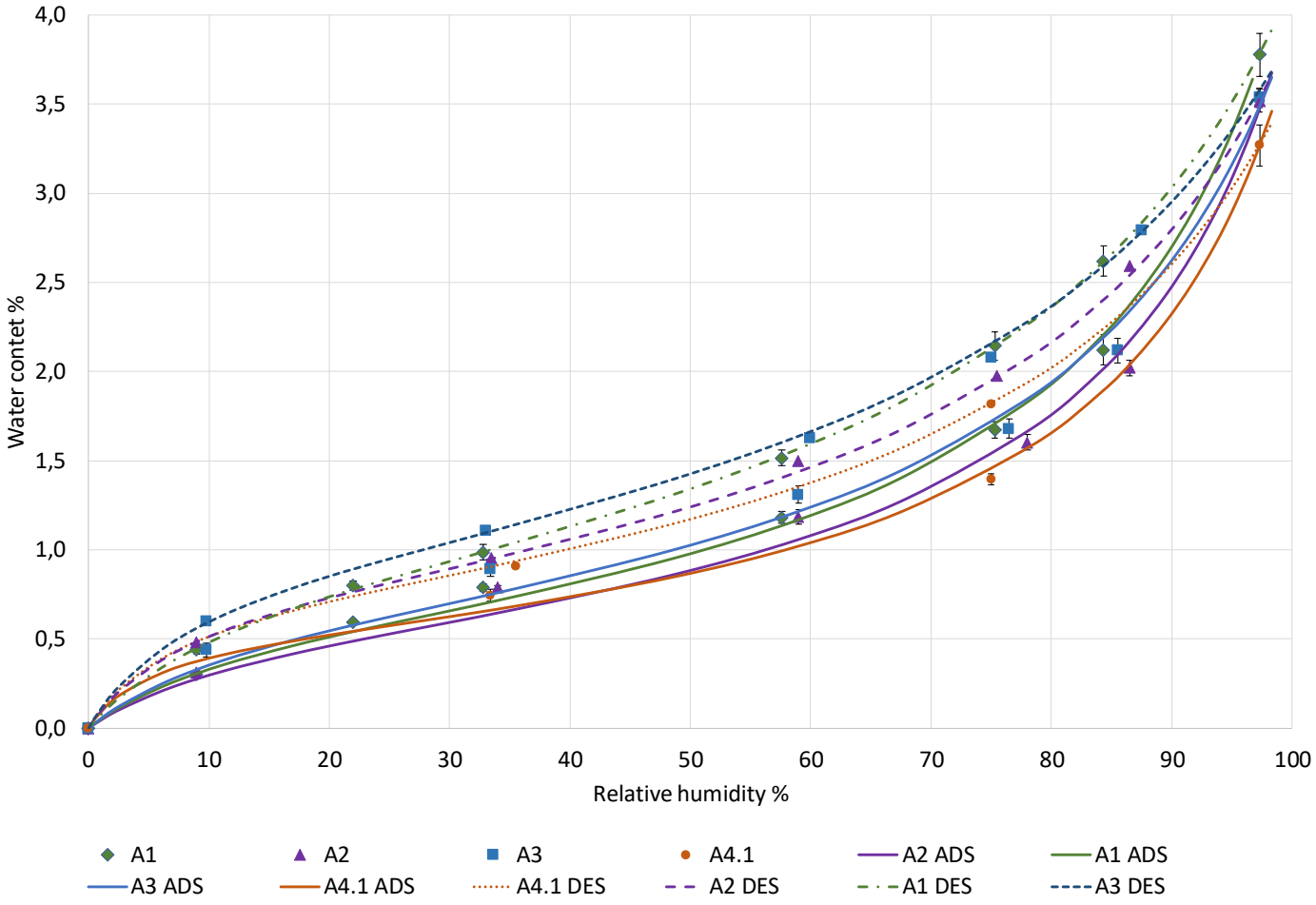

Figure 6 Sorption curves measured by SSS, measured points as average value are reported with the interpolated curve using GAB method and error bars are also reported. 'DES' stands for 'Desorption', 'ADS' stands for 'Adsorption'

Experimental points almost overlap from zero to 60%. For higher values of relative humidity, A1 samples show the highest moisture adsorption and A4.1 the lowest, but the difference remains limited and is close to the measurements' uncertainty. No clear behavior was identified between the samples' dry density and their maximal adsorption: A1 and A4.1 have a lower density (1855-1883 $kg.m^{-3}$) than samples A2 and A3 (2022-1943 $kg.m^{-3}$), but all of them present similar results. This observation is in accordance with the study by Zhang et al. [53] on compacted earthen bricks, where it is observed that the changes in the density only slightly impact the absorption of moisture. Indeed, the tested range of relative humidity corresponds to material microporosity, whereas compaction, which modifies the dry density, affects mainly the macroporosity.

The classical hypothesis is to consider that coarse particles do not participate in the phenomena of water sorption, while clay fraction is principally responsible for it, due to its high specific surface. Due to the

definition of moisture content as the ratio of water and dry mass weights, given by formula (1), the soil with higher content of clay is expected to adsorb more water compared to others [54]. Under this hypothesis, the adsorption curve of sample A4.1 (20 mm) is expected to be significantly lower than others, since 50% of the grain size distribution is composed of gravels not present in the soil sieved at 5 mm. Therefore, the same amount of water adsorbed by clay fraction, divided for a doubled total mass would give halved water content. (Figure 6). This is not the case in the present results, suggesting different hypothesis: gravel's interface with clay could participate in the sorption behavior, or gravel's presence could modify locally pore-size distribution.

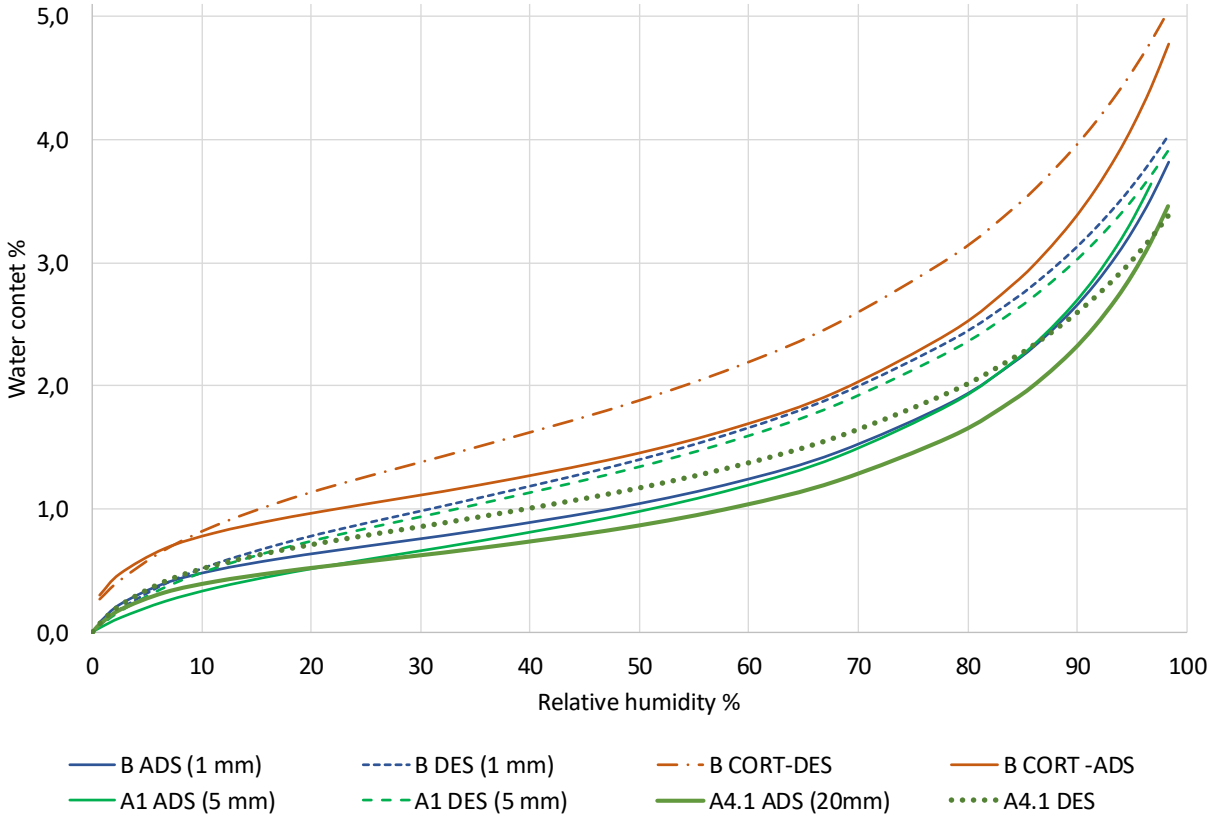

Figure 7 Comparison between different curves by SSS (A1, A4.1), DVS (B) and DVS with correction (B CORT). The maximal grain size for each test is also reported. 'DES' stands for 'Desorption', 'ADS' stands for 'Adsorption'.

Comparison between SSS and DVS

Figure 7 compares two curves by SSS (A1 and A4.1) to one curve by DVS (B). The correction on the different drying temperatures illustrated in equation (3) is applied to curve B to obtain curve B-CORT. The correspondence between curves B and A1 is quite precise for all values of RH%. The curve B-CORT is shifted

quite far from the others, suggesting that other factors may be considered in addition to this first correction, such as the different grain size distribution (1 mm B-CORT against 5 mm of A1 and 20 mm of A1.4). This element may explain the higher values of B-CORT, due to the higher percentage of clay with higher moisture adsorption. Conversely, as already mentioned, the difference between A1 and curve A1.4 is smaller, although the maximal grain size increases from 5 to 20 mm.

Figure 8 reports the quantification of the hysteresis as the difference in water content between the adsorption and desorption curves at equivalent RH, determinated from the interpolated curves. The hysteresis of the intermediate loop (C curve) is almost half of the complete sorption isotherm at 70%, showing a strong reduction of hysteresis for lower values of RH. Hysteresis curves determined by DVS seem to have a similar shape, with a peak around 85% RH and lower values at low RH% compared to the curves

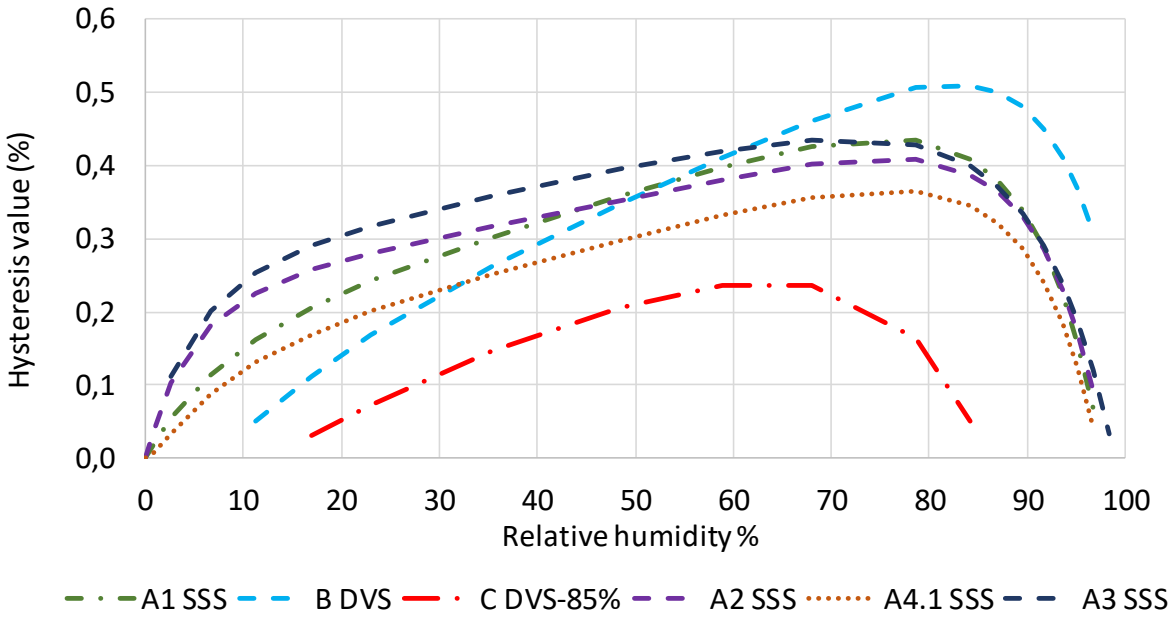

Figure 8 Hysteresis comparison of different sorption isotherms measured by DVS and SSS.

measured by SSS. This phenomenon may be due to the low number of points measured by SSS under 30% RH and the overall effect given by interpolation. The hysteresis increases when higher relative humidity is reached for curves up to 0.5%, in accordance with the results reported by Cangon et al. [55]. Among the curves by SSS, A4.1 presents slightly lower values compared to the others, probably due to the bigger grain size distribution of 20 mm compared to 5 mm.

As global results on sorption isotherm determination, SSS assures good repeatability for values of relative humidity lower than 60% (see whiskers in Figure 6). For higher values, the differences are slightly

higher but remain very limited. DVS technique uses only a few mg of soil for the test and it can be a faster way to represent the behavior of bigger samples, although further investigations are needed on the methods to compare the initial mass of the samples in the two tests. Furthermore, the equilibrium criterion on the mass variation used for DVS (C samples) in this case was 0.0005% par minute, while for SSS it was 0.01% at 48h. Another aspect that should be considered is the small quantity of soil used in the test. It has then a high probability of not being fully representative of the real soil composition since just a few milligrams are compared. The small differences in the curves can therefore be explained by the combination of all these factors.

3.2 Water vapor resistance factor μ

The vapor transfer is measured over an interval of two relative humidities (inside and outside the cup). Different batches of samples were used for the test, considering different dimensions (batches B2, B3, B4) and dry density (B1).

Laboratory B

The measurements were performed at high levels of relative humidity (between 80 and 97 %). The correction for the masked edge was applied at first following formula (8). The correction on the air layer resistance formula (11) was then applied as reported in Figure 9, where the surface resistance coefficient Z can be determined by the intercept of the curve, in this case, equal to $2.14 \cdot 10^{8}$ Pa.m².s.kg^{-1}. Figure 10 reports μ_{-m} corrected only for the masked edge and μ with the additional correction for the surface resistance (Z). It can be observed that the measured μ_{-m} still depends on the thickness of the samples, while the corrections for the surface resistance lead to more uniform values.

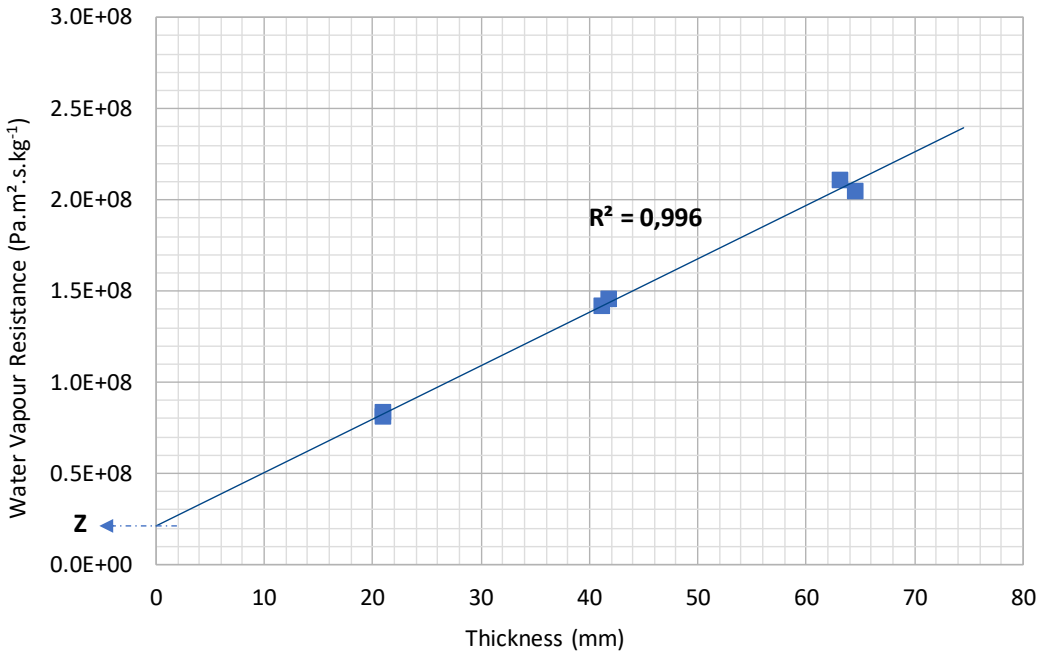

Figure 9. Global vapor transfer resistance for three different thicknesses of samples (batches B2, B3, B4).

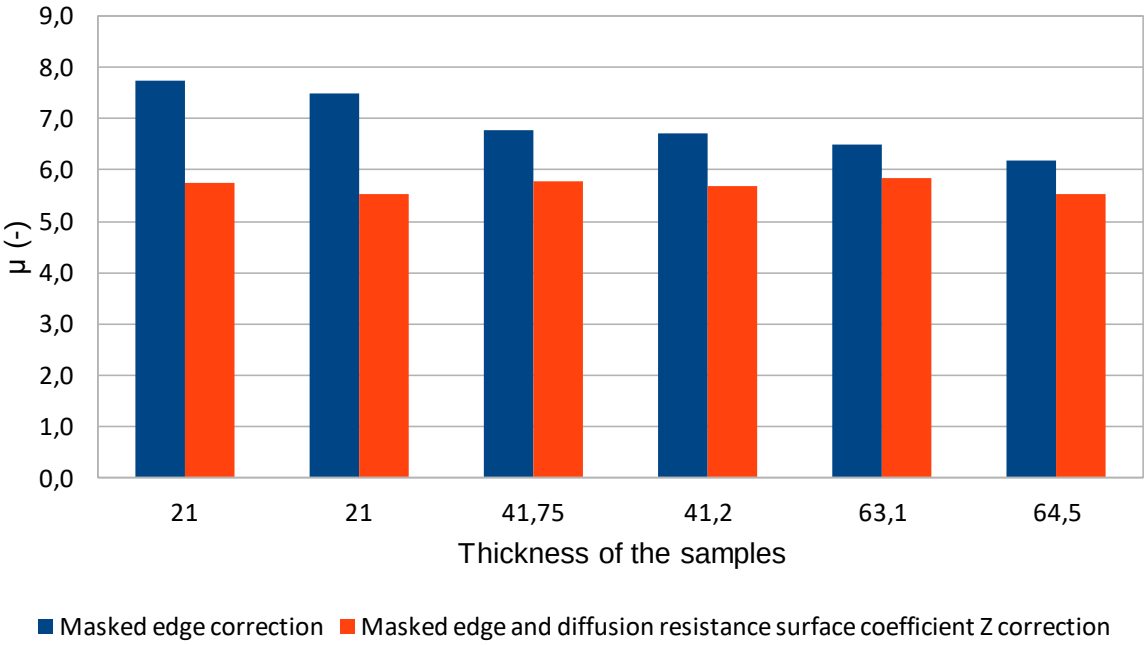

Figure 10 Vapor resistance factor using data corrected for masked edge (blue) and masked edge and surface diffusion resistance coefficient Z (red).

Here, the mean value of vapor resistance factor reported for a density of 1.66 is equal to 5.7, and for samples with a density of 1.93 is equal to 6.9. As expected, the specimens having a higher dry density also

have a higher resistance to vapor transfer due to the lower porosity (see also Chabriac, for soils with the same grain size distribution and a different porosity [12]).

Laboratory D

Table 4 reports the complete analysis of the results on wet and dry-cup for different intervals of relative humidity in laboratory D. The values measured are slightly higher than the common range in the literature for unstabilized RE materials, which can vary from 4 to 10 [-], due to higher density of the samples [56].

Table 4 Water vapor diffusion resistance factors measured at laboratory D.

RH in the cup.	RH in climatic chamber	Dry/wet	HR_avg	Sample 1 μ_1	Sample 2 μ_2	Average μ_ag	Standard deviation μ_st
11%	50%	Dry	31%	17.3	18.7	18.0	0.99
	85%	Dry	48%	13.80	-	13.8	0.00
50%	11%	Wet	30.5%	15.2	15.6	15.4	0.28
	85%	Dry	68%	12.7	-	12.7	0.00
85%	11%	Wet	48%	16.9	14.6	15.8	1.63
	50%	Wet	68%	12.7	-	12.7	0.00
0%	11%	Dry	5.5%	21	20	20.5	0.71
	50%	Dry	25%	18.9	18.3	18.6	0.42
	85%	Dry	42.5%	15.30	14.80	15.1	0.35

Comparison: Laboratories B & D

Samples B1 and D1 have a similar dry density of about 1985 kg.m^{-3} and are reported in Figure 11. As expected, the water vapor resistance factor μ measured at higher RH% presents lower values than μ measured at low RH%. Comparing all values, it is possible to find a linear interpolation between the RH% and μ (R^2=0.90). Medjelekh et al. [57] presented an exponential law to fit the measured values for the water content and water vapor permeability, but in the range between 0 and 2% of water content the dependence is almost linear, in accordance with the results presented above.

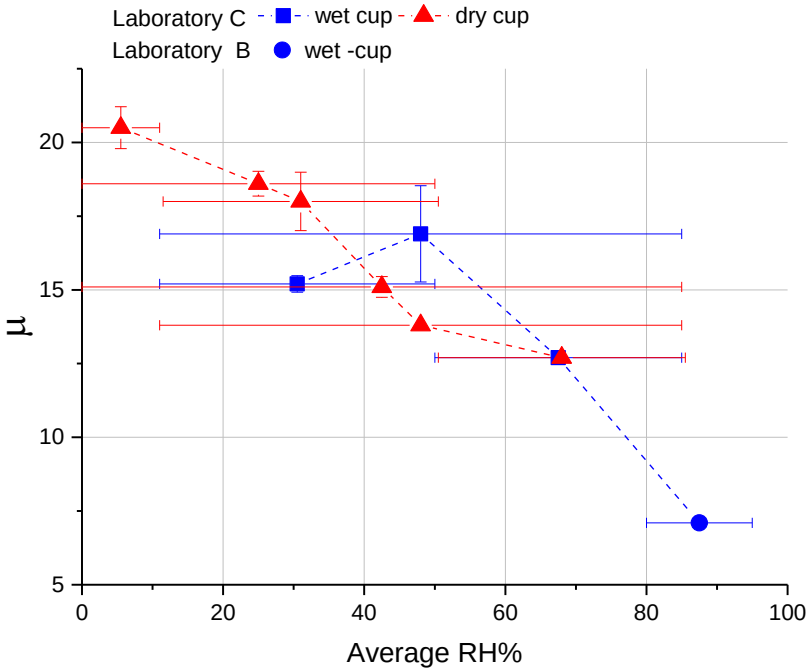

Figure 11 Summary graph with all data of wet-cup and dry-cup, considering the standard deviation of μ values (vertical whiskers) and the interval of RH on both sides of the samples (horizontal whiskers).

3.3 Specific heat capacity

The MDSC (Modulated Differential Scanning Calorimetry) gives an average specific heat capacity on three different samples. This value measured at 25 °C was 782 $J.kg^{-1}.K^{-1}$, in accordance with results from the literature which reports values between 684 and 939 $J.kg^{-1}.K^{-1}$ for RE materials [29]. The variation of the specific heat capacity depending on temperature is fully reported in paragraph 3.7.

3.4 Thermal conductivity, thermal diffusivity and effusivity – laboratory A and C

Two methods of measurement are used (C-Therm and Hot Disk) and two different laboratories performed the measurements as reported in Table 5. Before tests, the samples were conditioned at 58%. In addition to thermal conductivity, the diffusivity, effusivity and indirect calculation of specific heat capacity are compared to the reference value given by MDSC. Table 5 summarizes the results, all done on A3 batch.

*Table 5 Thermal conductivity results. Values with the * are calculated and not directly measured by the device.*

Laboratory/ technique	A/C-Therm	A/Hot Disk	C/Hot Disk	A/MDSC
Number of samples	2	4	6	3
Number of repetitions	4	4	4	1
Thermal conductivity ($W.m^{-1}.K^{-1}$)	1.380±0.065	1.275 ± 0.053	1.274 ± 0.053	-
T°C	25°C/28°C	22°C	26°C	-
Cp ($J.Kg^{-1}.°K^{-1}$)	*969 ± 3	*749±2	*692±2	782.3
Effusivity ($W.s^{0.5}.m^{-2}.K^{-1}$)	1648 ± 35	*1393	*1339 ±8	-

Diffusivity ($mm^2.s^{-1}$)	*0.700 ± 0.036	0.837 ± 0.033	0.906 ± 0.037	-

The thermal conductivity is calculated as the average of 4 measurements done on at least 2 samples or pairs of samples in the case of the Hot Disk. The values found at laboratory A (1.273 $W.m^{-1}.K^{-1}$) and laboratory C (1.274 $W.m^{-1}.K^{-1}$) by using the Hot Disk have a very low difference of 0.09%, assuring a good level of reproducibility. The measurements done with the C-therm show a slightly higher value around 1.380 $W.m^{-1}.K^{-1}$. The difference may be due to different contact between the surface and the sensor. In the case of Hot Disk, both sides of the sensor are in contact with the samples, while for the C-Therm there is a contact liquid (grease) which ensures the absence of voids between the sensor and the sample.

The thermal effusivity of RE was measured experimentally by C-Therm and found equal to 1648 $W.s^{0.5}.m^{-2}.K^{-1}$, greater than the values obtained by calculations from the Hot Disk measurements equal to 1339 $W.s^{0.5}.m^{-2}.K^{-1}$and 1393 $W.s^{0.5}.m^{-2}.K^{-1}$. The specific heat capacity estimated by the Hot Disk is about 11% lower than the one measured by MSDC and the overestimation is even larger in the case of C-term. In fact, the producer of the Hot Disk notifies that the calculated value of heat capacity is not reliable for heterogeneous materials as RE, but it can give correct information of the order of magnitude. Finally, the thermal diffusivity values calculated by Hot Disk are higher by 30% (lab A, 0.837 $mm^2.s^{-1}$ and lab C, 0.906 $mm^2.s^{-1}$) than the values obtained experimentally from C-Therm (0.7 $mm^2.s^{-1}$).

3.5 Thermal conductivity dependence on moisture content

Thermal conductivity at different moisture contents was measured for two types of samples with higher density (A2, 2022 $kg.m^{-3}$) and slightly lower density (A3, 1943 $kg.m^{-3}$). The results of the thermal conductivity are reported as an average value of 8 repeated measurements, done with Hot Disk on two pairs of samples (Figure 12). The standard deviation between the 8 measurements was always lower than the measurement error of Hot Disk apparatus equal to 5%. The latter is therefore reported on the graph.

The measured dry thermal conductivity λ_{dry} is about 1.39 $W.m^{-1}.K^{-1}$ for A2 samples and 1.19 $W.m^{-1}.K^{-1}$ for A3 samples, confirming that the change of the density impacts the thermal conductivity, as already shown for example by Zhang et al [53]. In our case, a difference of 4% in the density results in a difference in thermal conductivity of about 17%. These values are slightly high for RE materials as compared to the literature, which

often reports values around 0.2-1.1 $W.m^{-1}.K^{-1}$ [29,47,53,56]. This is probably due to the higher density of the present samples.

Figure 12 left reports the results of thermal conductivity versus relative humidity. A2 samples were measured for 7 levels of relative humidity during the adsorption and 2 levels during the desorption. The A3 samples were measured during the adsorption phase, at 6 different levels of relative humidity. The increment of thermal conductivity is about +19% from 0 to 75% RH, while at 97% RH it is +39% compared to λ_{dry} (A2 samples). The disposition of the values reproduces the shape of the sorption curve. The values measured in the desorption phase are slightly higher compared to the values measured during the adsorption (about 0.05 $W.m^{-1}.K^{-1}$), indicating the influence of the hysteresis already investigated by the sorption isotherm.

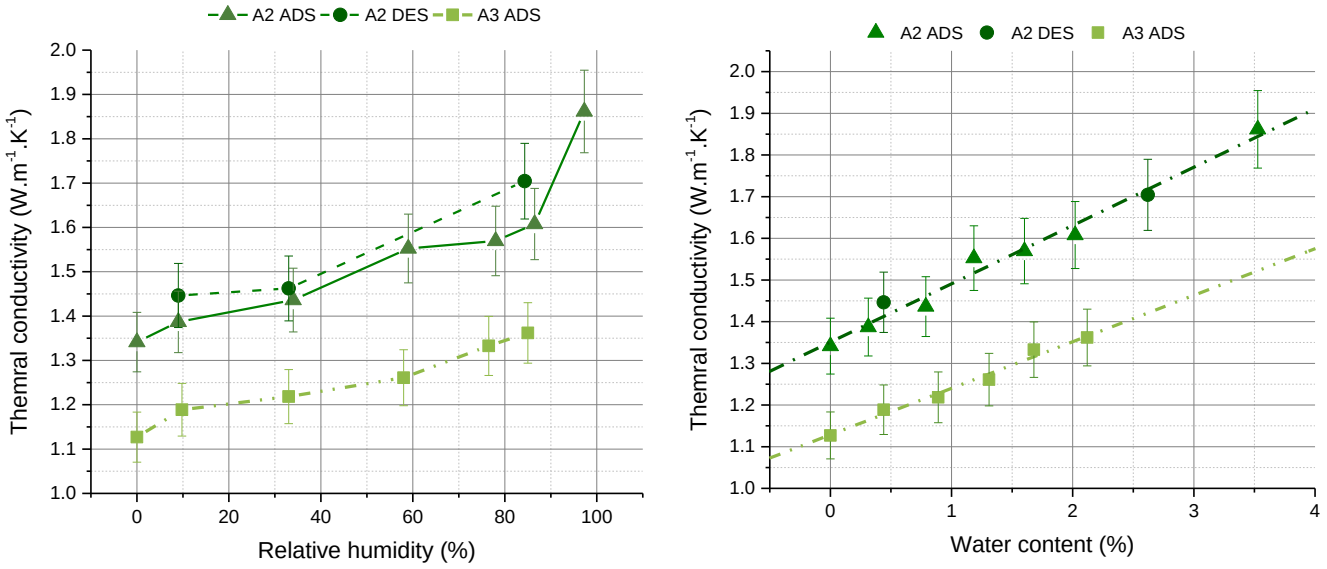

Figure 12 Thermal conductivity versus relative humidity in samples A2 and A3 both during adsorption (ASD) and desorption (DES) (left). Thermal conductivity versus water content (right).

Using sorption isotherm, the thermal conductivity was plotted versus the corresponding water content, showing the expected linear behavior (Figure 12 right). The linear correlation coefficient R^2 is about 0.98 for both types of samples. Moisture-dependent thermal conductivity (λ_w) shows a linear dependency on moisture content as already confirmed for RE materials by different authors [12,27,47,58]. A possible formulation inspired by the model cited by Soudani, Labat and Kunzel [24,47,59–62] to describe this behavior using an empiric mode is here reported :

$$\lambda_w = \lambda_{dry} + C_s \cdot w \tag{22}$$

Where λ_{dry} is the dry thermal conductivity, w the gravimetric moisture content as a percentage (% kg.kg^{-1}) and C_s (W. m^{-1}K^{-1}) a constant characteristic of the soil. A similar formulation proposed by Künzel [24] and implemented in WUFI® to determine material's properties is reported in formula (23):

$$\lambda_w = \lambda_{dry}(1 + b \cdot w_{fr}) \quad (23)$$

Where w_{fr} is the gravimetric moisture content as a fraction (kg.kg^{-1}) b (%/M-%) is the thermal conductivity supplement, defined as the percentage of the thermal conductivity increase per mass percentage of moisture [24,61,62]. This coefficient must be measured for each type of building material and it is related to C_s as follows:

$$b = \frac{C_s}{\lambda_{dry}} * \mathbf{100} \quad (24)$$

Since both models presented above require the determination of coefficients (λ_{dry}, C_s and b) that depend on the type of the soil, a further investigation on a larger batch of soils is here presented to evaluate the possibility of approximating these values for RE materials and avoiding long and demanding experimental measurements.

Approximations of moisture-dependent thermal conductivity coefficients

Limiting the field of investigation to unstabilized RE materials, a wider batch of experimental measurements were identified in the literature analyzing the relationship between moisture content and thermal conductivity. Table 6 reports thermal conductivity data for 6 different unstabilized REs: Chabriac [12] (soils from Lyon and Monteserveoux, France), Tan et al. [63] (soil from Mianyang, China), Soudani [47] (soil from St Antoine l'Abbey, France) and Losini et al. [25] (Lozzolo, Italy). The tests were executed using hot-wire or Hot Disk methods, on RE samples. Table 6 reports the dry density, porosity and λ_{dry} for the different soils. The linear interpolation for each soil (following equation 25) presents a satisfying R^2 value and C_s is determined between 0.086 and 0.14 W. m^{-1}K^{-1} for 5 out of 6 soils investigated, while the soil from Mianyang, China, presents a lower value equal to 0.03 W. m^{-1}K^{-1} (Table 6) [63]. Although this RE has a density of 2100 kg.m^{-3} and a compressive strength of 2 MPa, similar to the soil from Lozzolo, its thermal conductivity increases at a much lower rate. Differences in soil composition could be a reason, but the article gives no further information.

In order to compare the variability of λ with water content, independently from the earth studied, $\lambda - \lambda_{dry}$ (that is to say $C_s.w$) is plotted as a function of w in Figure 13. The linear interpolation of all the values presents an R^2 equal to 0.99 and a global C_s coefficient equal to 0.089 W. $m^{-1}K^{-1}$, except for Mianyang soil.

Table 6 presents also a calculation of thermal conductivity supplement *b* for the different RE materials. The WUFI® library and literature report different values for different materials: around 8 for concrete, gypsum and clay rendering, 4 for cellular concrete and aerated clay bricks, 3.34 for hempcrete and 1.5 for wood [24,62,64]. The values found in the present study, around 9 for both samples A2 and A3, are aligned with the values presented in the literature. Soils investigated in the literature present higher values, between 14 and 16, except for the soil of Mianyang, which stays around 5.

Considering the prediction of λ_{dry}, the relationship between the density and the dry thermal conductivity is not easily predictable when changing grain size distribution and clay mineral composition in the soil, probably due to the modification of the complex porous network. In fact, different studies on a larger batch of soils report a general trend that relates higher thermal conductivity to higher dry density, but with a low linear correlation coefficient R^2 of around 0.8-0.6 [12,53]. Therefore, the dry thermal conductivity of RE should be measured for each soil composition.

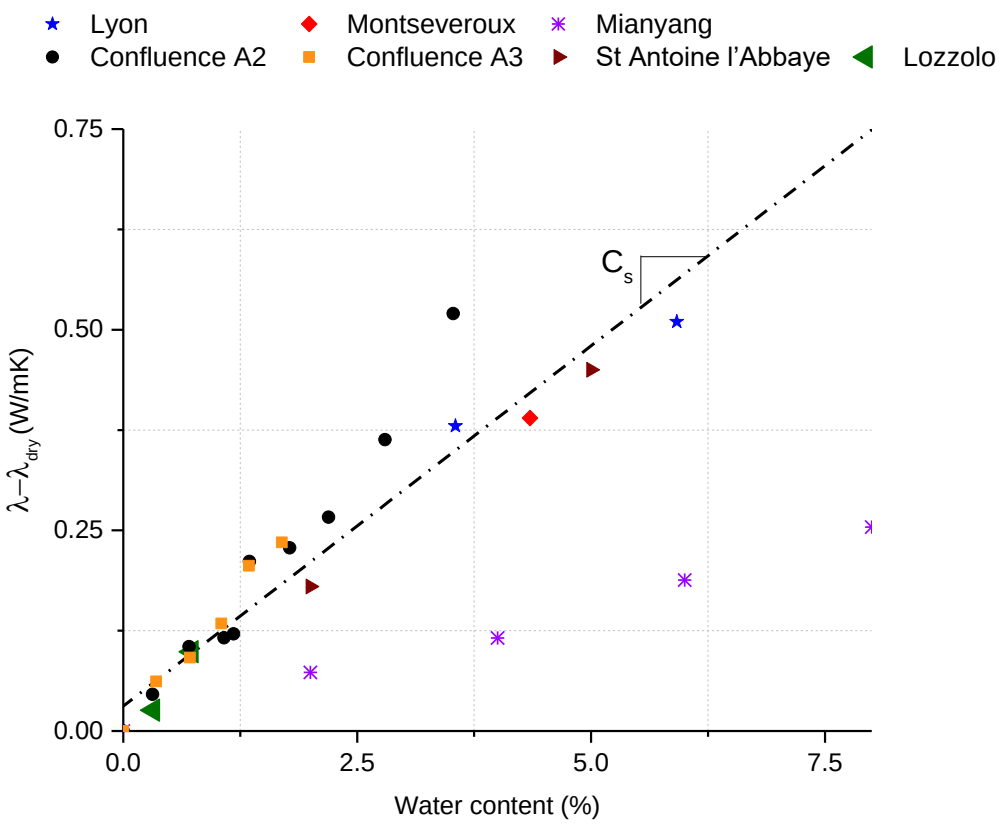

Figure 13 Thermal conductivity plotted versus water content, considering also the slope.

Table 6 Data from literature and the present study. The type of samples and device used in the test are reported, with the dry density, porosity, dry thermal conductivity, Cs and R^2 from the linear interpolation of λ_w. Thermal conductivity supplement b is also reported and the reference of the study.

RE	Samples	Device	Υ_d ($g.cm^{-3}$)	N (-)	λ_{dry} ($W.m^{-1}.K^{-1}$)	Cs ($W.m^{-1}.K^{-1}$)	R^2	b (%/M-%)	Ref.
St Antoine	CEB	Hot-wire	1.73	0.35	0.64	0.09	0.99	14.06	[12,47]
Lozzolo	4x4x3.5	Hot Disk	2.1	0.21	1.435	0.14	0.93	9.06	[65]
Confluence A2	Ø=7 h=1.5	Hot Disk	2.02	0.25	1.34	0.14	0.97	8.96	-
Confluence A3	Ø=10 h=2	Hot Disk	1.94	0.27	1.13	0.14	0.98	8.85	-
Lyon	CEB	Hot-wire	1.62	0.39	0.57	0.09	0.99	15.79	[12]
Montrservoux	CEB	Hot-wire	1.62	0.39	0.61	0.09	0.99	14.75	[12]
Mianyang	Ø=7 h=2	Hot Disk	2.1	0.21	0.53	0.03	0.99	5.66	[63]

3.6 Liquid transport suction and redistribution coefficients

The values obtained for the water absorption coefficient$_{-value}$ in laboratory B are equal to 0.160 ± 0.02 kg.m^{-2}.s $^{-1/2}$ congruent with literature, between 0.26 to 0.6 kg.m^{-2}.s$^{-1/2}$ [31,48]. The values obtained by laboratory A are slightly lower, around 0.20 ± 0.002 kg.m^{-2}.s $^{-1/2}$. The different results can be due to the different sample sizes, the modified grain size distribution and the test configuration [31]. The smaller B5 samples were in direct contact with water and the total test time (1h) was used to determine the linear uptake of water. The bigger A4 sample has a longer test time due to its larger size and the indirect contact with water using fine sand. In this case, only the first 15 minutes of the 17-day test were used.

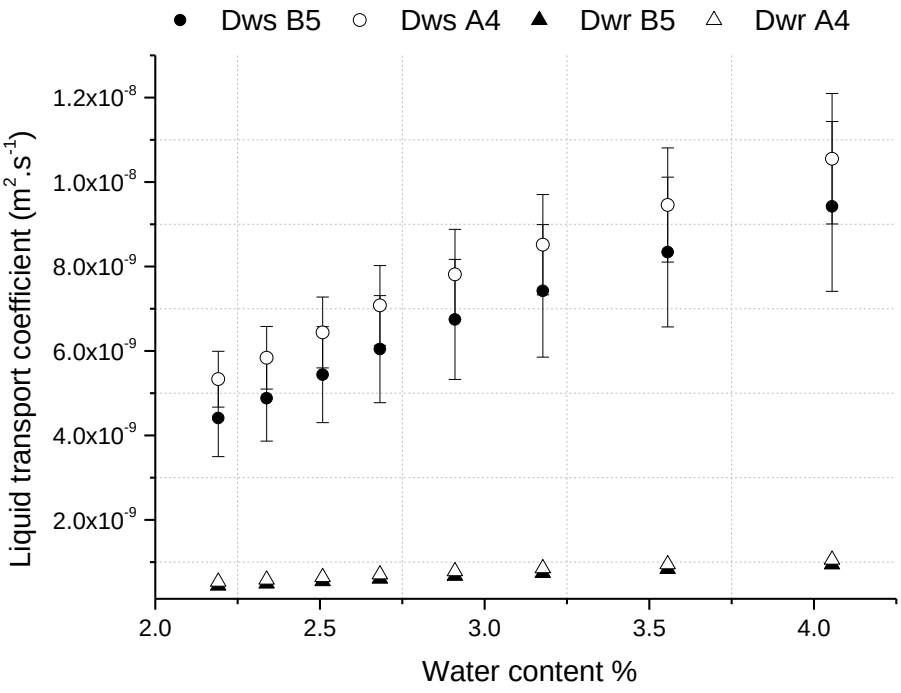

Figure 14 Liquid transport coefficient for suction (Dωs) and redistribution (Dωr).

Using a theoretical value of ω_f equal to 267 kg.m^{-3} and 289 kg.m^{-3} for respectively B5 and A4 samples, ρ_s equal to 2,650 kg.m^{-3}, ρ_l equal to 1,000 kg.m^{-3}, liquid transport coefficient for suction $D_{\omega s}$ (m².s^{-1}) was calculated using equations 23 and 19. The values of the liquid transport coefficient for suction are between 4.4·10^{-9} and 1·10^{-8} m².s^{-1}, as reported in Figure 14. Samples A4 show higher values compared to samples B5, probably due to the different A_{-value} and dry density of the samples (1940 kg.m^{-3} and 1883 kg.m^{-3} respectively for B5 and A4). The liquid transport coefficient for redistribution $D_{\omega r}$ (m².s^{-1}) can be calculated as one decimal

power below the liquid transport coefficient for suction [24] (Figure 14). The results are in accordance with literature, which reports around 10^{-12} m².s^{-1} for cellular concrete and 10^{-8} m².s^{-1} for plasterboard for D_{ws}.

3.7 Summary table of hygrothermal properties for modeling

Table 7and Table 8 propose a summary of all values presented in this article adapted to be used for combined heat and moisture transfer simulations in Kunzel model, implemented in WUFI® and EnergyPlus™ [24,25,66]. This data set could be considered representative of the material properties of the blocks used for the building *l'Orangerie*, made with an average dry density of 1930 kg.m^{-3}, similar to the samples prepared in this study. The results are reported depending on the percentage gravimetric water content w (% kg.kg^{-1}) or relative humidity (%). Often the models require the input as relative humidity fraction (-) and mass par volume water content ω (kg.m^{-3}). In this case, the density of the building blocks (1930 kg.m^{-3}) was considered for conversion, except in the case of thermal conductivity for low and high density samples. Generally, the models are not able to consider the effect of the hysteresis. An average between adsorption and desorption values is proposed, considering the sorption isotherm of samples A1 measured using SSS and interpolated using GAB method. For higher detail of investigation, boths sorption and desorption measured values are report also reported, always for A1 samples. The values of water vapor resistance factor, measured on an interval of RH, are referred to using the average value of RH to represent the interval. For the thermal conductivity, two possibilities are proposed, for low and high-density material, inspired by the samples A2 and A3 tested in the article. For the liquid transport coefficients (suction and redistribution), the values from the capillary rise test of sample B5 are preferred, as B5 sample has the same grain size distribution as the building blocks, with a similar density (1940 kg.m^{-3}).

Table 7 Data of density, porosity and thermal conductivity for the different samples measured with high and low dry density, compared with the RE building l'Orangerie.

Field	Unit	RE High density (A2)	RE Low density (A3)	RE Building
Dry Density ρ_d	kg.m^{-3}	2022	1943	1930
Porosity	-	0.25	0.27	-
Dry thermal conductivity	W.mK^{-1}	1.34	1.13	-

*Table 8 Moisture-dependent parameters for heat and moisture transfer simulations. Some data are reported in case of low (l) or high (h) density material. In water vapor resistance factor all dry-cup values are reported except for the value at *88% RH.*

Non-constant parameters for heat and moisture transfer simulation											
Average of adorption/desorption isotherm – GAB interpolation (A1)											
RH	(%)	9	22.93	35.42	48.51	58.96	68.08	78.63	84.2	89.54	98.36
w	(%)	0.44	0.68	0.89	1.13	1.37	1.64	2.08	2.40	2.82	3.92
ω	($kg.m^{-3}$)	8.49	13.12	17.17	21.80	26.44	31.65	40.14	46.32	54.42	75.66

Adsorption(ADS)/desorption (DES) isotherm experimental points (A1)								
RH	(%)	9.00	22.00	32.80	57.60	75.30	84.34	97.30
w_ADS	(%)	0.30	0.59	0.79	1.18	1.67	2.12	3.78
ω_ADS	($kg.m^{-3}$)	5.76	11.44	15.22	22.79	32.31	40.93	72.92
w_DES	(%)	0.44	0.80	0.98	1.51	2.14	2.62	3.78
ω_ADS	($kg.m^{-3}$)	8.51	15.39	19.00	29.24	41.36	50.56	72.92

Water vapor resistance factor (D1, B4)								
RH	(%)	5.5	25	31	42.5	48	68	88*
μ	(-)	20.5	18.6	18	15.1	13.8	12.7	7.05

Moisture-dependent thermal conductivity low and high density (A3, A2)							
(A3)	RH%	0	9.8	33.4	59	76.5	85.50
w_l	(%)	0	0.44	0.89	1.31	1.68	2.12
ω _l	($kg.m^{-3}$)	0.00	8.55	17.29	25.45	32.64	41.19
λw_l	($W.m^{-1}.K^{-1}$)	1.13	1.19	1.22	1.26	1.33	1.36
(A2)	RH%	0	9	34	59	78	86.5	97.3
w_h	(%)	0	0.31	0.79	1.18	1.60	2.02	3.53
ω _h	($kg.m^{-3}$)	0	6.27	15.97	23.86	32.35	40.84	71.38
λw_h	($W.m^{-1}.K^{-1}$)	1.34	1.39	1.44	1.55	1.57	1.61	1.86

Specific Heat capacity										
T	°C	10	15	20	25	30	35	40	45	50
c	$J.kgC^{-1}$	747	763	773	782	791	799	808	818	827

Liquid water transport coefficient - suction $D_{ωs}$ and redistribution $D_{ωr}$									
RH	(%)	84.20	86.98	89.54	91.68	93.63	95.12	96.73	98.36
w	(%)	2.40	2.61	2.82	3.03	3.25	3.44	3.68	3.92
ω	($kg.m^{-3}$)	4.64	5.03	5.45	5.85	6.28	6.64	7.09	7.56
$D_{ωs}$	$\cdot 10^{-9}$ ($m^2.s^{-1}$)	4.41	6.64	5.44	6.04	6.75	7.42	8.34	9.42
$D_{ωr}$	$\cdot 10^{-10}$ ($m^2.s^{-1}$)	4.41	6.64	5.44	6.04	6.75	7.42	8.34	9.42

4 Conclusions

The present work reports the results of a large collaboration of four academic laboratories aiming at an extensive hygrothermal characterization considering moisture-dependent parameters of rammed earth materials used in modern construction. A complete data set for the same type of rammed earth is presented and adapted for combined heat and moisture transfer modeling. The use of DVS and SSS methods gives similar adsorption/desorption isotherms curves. As a surprising result, variations in the grain size distribution

do not produce a significant modification in the adsorption/desorption isotherms, while hysteresis slightly reduces when bigger grains are added to the soil composition. Hysteresis almost doubles at 70% comparing samples that undergo 97% RH compared to 84% RH. Experimental results show how variations in the density of the samples do not impact significantly the sorption isotherm. Conversely, density variation has an important impact on thermal conductivity and water vapor resistance factors. The vapor transfer resistance factor was determined for a large span of relative humidity using both dry and wet-cup methods.

The use of Hot Disk apparatus for thermal conductivity measurements shows excellent reproducibility. Conversely, the use of C-Therm device for materials with a rough surface and higher thermal conductivity such as rammed earth seems more complex, due to the necessity of using a contact agent to provide a good contact surface while maintaining stable humidity in the sample. MDSC provides direct measurements of specific heat capacity and should be preferred to indirect calculations from Hot Disk and C-Therm which presented a minimum overestimation of 11%. Linear correlation was verified between moisture content and λ_w, moisture-dependent thermal conductivity. Satisfying R^2 coefficients (>0.97) are obtained using empirical linear models in which appears two parameters: dry thermal conductivity λ_{dry} and C_s coefficient related to the specific type of rammed earth. Despite the experimental measurement of λ_{dry} are always necessary, a first approximation of C_s is proposed for different rammed earth materials.

The presented results provide a complete data set of hygrothermal data, approaching some difficulties and issued related to adapting the hygrothermal measurement techniques to a non-standardized material such as rammed earth. For future investigation, it should be reminded that using data measured in the laboratory at the material scale to simulate physical properties at the building scale is a common practice, but there are concerns about the changes in scale due to the heterogeneity of soil. In particular, further investigations are suggested to evaluate the impact of varying grain size distribution when measuring hygrothermal properties, considering related modifications in the density, pore size distribution and not less important roughness in the surface that bigger particles produce. These modifications may affect the different hygrothermal properties, suggesting that in some cases laboratory investigations need corrections to consider scale effects, that for the moment are not yet clearly identified.

Author Contributions: Investigation A.E.L., S.O., D.G., J.O., T.C., J.O., D.G,; Grain size distribution T.C. Investigation sorption isotherm. A.E.L. T.C., S.O.; Investigation water vapor permeability M.D., D.G, A.P.-P.; Investigation thermal conductivity A.E.L.,; Investigation capillary rise T.C., A.P., Formal analysis. A.E.L., M.W., S.O, A.P.-P., T.C., M.S., N.P., T.C.; Methodology A.E.L., M.W., S.O., R.R., A.P.-P., T.C., M.S., N.P.; Data curation, A.E.L., M.S., T.C,; Original draft A.E.L.; review and editing. A.E.L., M.W., N,P, M.S.F., A.P.-P., M.D., S.O., R.R.; visualization. A.E.L., T.C., S.O., A.P-P.,; supervision. N.P., M.W., R.R., and A.-C.G.; project administration. N.P., M.W. and A.-C.G.; funding acquisition. N.P., A.-C.G. and M.W.; conceptualization A.E.L., M.W.,R.R., A.-C.G. All authors have read and agreed to the published version of the manuscript.

Funding: This research was financed by VBATCH ANR (18-CE22-0007), TERAC project (ADEME) and Supported by Smart-Reno project (grant Certificat Economie d'Energie, CEE, operated by ADEME), and by the French National Research Agency, through Investments for Future Program (ref. ANR-18-EURE-0016 - Solar Academy).

Institutional Review Board Statement: Not applicable. Informed Consent Statement: Not applicable.

Acknowledgments: The authors would thank Antonin Fabbri, Laura Leteve, Aude Sini and Stephane Cointet for their support in the experimental activities and Olivier Plé for critical discussions.

Bibliography

[1] IEA, World Energy Outlook 2022, International Energy Agency, 2022. https://www.iea.org/Reports/World-Energy-Outlook-2022/Executive-Summary.

[2] G.L.F. Benachio, M. do C.D. Freitas, S.F. Tavares, Circular economy in the construction industry: A systematic literature review, J. Clean. Prod. 260 (2020) 121046. https://doi.org/10.1016/j.jclepro.2020.121046.

[3] M.K. Dixit, Life cycle recurrent embodied energy calculation of buildings: A review, J. Clean. Prod. 209 (2019) 731–754. https://doi.org/10.1016/j.jclepro.2018.10.230.

[4] J.C. Morel, A. Mesbah, M. Oggero, P. Walker, Building houses with local materials: means to drastically

reduce the environmental impact of construction, Build. Environ. 36 (2001) 1119–1126. https://doi.org/https://doi.org/10.1016/S0360-1323(00)00054-8.

[5] T. getty conservaiton Institute, The earthen architecture initiative: guidelines for the teaching of earthen conservation. Materials analysis - earthen construction techniques, 2011.

[6] A.T.M. Marsh, Y. Kulshreshtha, The state of earthen housing worldwide: how development affects attitudes and adoption, Build. Res. Inf. 50 (2022) 485–501.

[7] S.E. Hale, A.J. Roque, G. Okkenhaug, E. Sørmo, T. Lenoir, C. Carlsson, D. Kupryianchyk, P. Flyhammar, B. Žlender, The reuse of excavated soils from construction and demolition projects: Limitations and possibilities, Sustain. 13 (2021) 1–15. https://doi.org/10.3390/su13116083.

[8] F. Pacheco-Torgal, S. Jalali, Earth construction: Lessons from the past for future eco-efficient construction, Constr. Build. Mater. 29 (2012) 512–519. https://doi.org/10.1016/j.conbuildmat.2011.10.054.

[9] A. Pelé-Peltier, A. Fabbri, J.C. Morel, E. Hamard, M. Lhenry, A similitude relation to assessing the compressive strength of rammed earth from scale-down samples, Case Stud. Constr. Mater. 16 (2022). https://doi.org/10.1016/j.cscm.2022.e00921.

[10] S. Sposito, F. Scalisi, Sustainable architecture: the eco-efficiency earth construction, Eur. J. Sustain. Dev. 6 (2017) 246–254. https://doi.org/10.14207/ejsd.2017.v6n4p246.

[11] F. McGregor, A. Heath, A. Shea, M. Lawrence, The moisture buffering capacity of unfired clay masonry, Build. Environ. 82 (2014) 599–607. https://doi.org/10.1016/j.buildenv.2014.09.027.

[12] P. Chabriac, Mesure du comportement hygrothermique du pisé, Thesis at University of Lyon, 2014. https://hal.archives-ouvertes.fr/tel-01413611.

[13] L. Ben-Alon, A.R. Rempel, Thermal comfort and passive survivability in earthen buildings, Build. Environ. (2023) 110339.

[14] A. Bassoud, H. Khelafi, A.M. Mokhtari, A. Bada, Evaluation of summer thermal comfort in arid desert areas. Case study: Old adobe building in Adrar (South of Algeria), Build. Environ. 205 (2021) 108140. https://doi.org/10.1016/j.buildenv.2021.108140.

[15] J. Fernandes, R. Mateus, H. Gervásio, S.M. Silva, L. Bragança, Passive strategies used in Southern

Portugal vernacular rammed earth buildings and their influence in thermal performance, Renew. Energy. 142 (2019) 345–363. https://doi.org/10.1016/j.renene.2019.04.098.

[16] G. Minke, Building with earth, Design and Technology of a Sustainable Architecture, Birkhäuser – Publishers for Architecture, 2012.

[17] M. Woloszyn, T. Kalamees, M.O. Abadie, M. Steeman, A. Sasic Kalagasidis, The effect of combining a relative-humidity-sensitive ventilation system with the moisture-buffering capacity of materials on indoor climate and energy efficiency of buildings, Build. Environ. 44 (2009) 515–524. https://doi.org/10.1016/j.buildenv.2008.04.017.

[18] A. Pelé-Peltier, R. Charef, J.-C. Morel, Factors affecting the use of earth material in mainstream construction: a critical review, Build. Res. Inf. 51 (2023) 119–137.

[19] P. Chauhan, A. El Hajjar, N. Prime, O. Plé, Unsaturated behavior of rammed earth: Experimentation towards numerical modelling, Constr. Build. Mater. 227 (2019) 116646. https://doi.org/10.1016/j.conbuildmat.2019.08.027.

[20] M. Woloszyn, C. Rode, IEA Annex 41 , MOIST-ENG Modelling Principles and Common Exercises -Final Report, IEA ECBCS Annex 41 Subtask 1 Rep. (2007) 1–161.

[21] J. Goffart, M. Rabouille, N. Mendes, Uncertainty and sensitivity analysis applied to hygrothermal simulation of a brick building in a hot and humid climate, J. Build. Perform. Simul. 10 (2017) 37–57. https://doi.org/10.1080/19401493.2015.1112430.

[22] T. Busser, J. Berger, A. Piot, M. Pailha, M. Woloszyn, Dynamic experimental method for identification of hygric parameters of a hygroscopic material, Build. Environ. 131 (2018) 197–209. https://doi.org/https://doi.org/10.1016/j.buildenv.2018.01.002.

[23] L.M. Lalicata, A.W. Bruno, D. Gallipoli, Hygro-thermal coupling in earth building materials, in: E3S Web Conf., 2023: pp. 1–6. https://doi.org/10.1051/e3sconf/202338223003.

[24] H.M. Künzel, Simultaneous Heat and Moisture Transport in Building Components One- and two-dimensional calculation using simple parameters ., 1995.

[25] A.E. Losini, A.-C. Grillet, L. Vo, G. Dotelli, M. Woloszyn, Biopolymers impact on hygrothermal properties of rammed earth : from material to building scale, Bulging Environ. 233 (2023) 110087.

https://doi.org/10.1016/j.buildenv.2023.110087.

[26] M. Labat, C. Magniont, N. Oudhof, J.-E.E. Aubert, From the experimental characterization of the hygrothermal properties of straw-clay mixtures to the numerical assessment of their buffering potential, Build. Environ. 97 (2016) 69–81. https://doi.org/https://doi.org/10.1016/j.buildenv.2015.12.004.

[27] M. Hall, D. Allinson, Analysis of the hygrothermal functional properties of stabilised rammed earth materials, Build. Environ. 44 (2009) 1935–1942. https://doi.org/10.1016/j.buildenv.2009.01.007.

[28] A.E. Losini, A.C. Grillet, M. Bellotto, M. Woloszyn, G. Dotelli, Natural additives and biopolymers for raw earth construction stabilization – a review, Constr. Build. Mater. 304 (2021) 124507. https://doi.org/10.1016/j.conbuildmat.2021.124507.

[29] G. Giuffrida, R. Caponetto, F. Nocera, Hygrothermal properties of raw earth materials: A literature review, Sustain. 11 (2019). https://doi.org/10.3390/su11195342.

[30] M.L. Indekeu, H. Janssen, M. Woloszyn, Determination of the moisture diffusivity of rammed earth from transient capillary absorption moisture content profiles, Constr. Build. Mater. 318 (2022). https://doi.org/10.1016/j.conbuildmat.2021.125978.

[31] M.L. Indekeu, C. Feng, H. Janssen, M. Woloszyn, Experimental study on the capillary absorption characteristics of rammed earth, Constr. Build. Mater. 283 (2021) 1–24. https://doi.org/10.1016/j.conbuildmat.2021.122689.

[32] V. Cascione, D. Maskell, A. Shea, P. Walker, A review of moisture buffering capacity: From laboratory testing to full-scale measurement, Constr. Build. Mater. 200 (2019) 333–343. https://doi.org/10.1016/j.conbuildmat.2018.12.094.

[33] A. Arrigoni, A.C. Grillet, R. Pelosato, G. Dotelli, C.T.S. Beckett, M. Woloszyn, D. Ciancio, Reduction of rammed earth's hygroscopic performance under stabilisation: an experimental investigation, Build. Environ. 115 (2017) 358–367. https://doi.org/10.1016/j.buildenv.2017.01.034.

[34] T. Chitimbo, N. Prime, O. Plé, F. Abdulsamad, Drying experiment on rammed earth structure, Eur. J. Environ. Civ. Eng. 0 (2022) 1–17. https://doi.org/10.1080/19648189.2022.2099983.

[35] A. Fabbri, F. McGregor, I. Costa, P. Faria, Effect of temperature on the sorption curves of earthen

materials, Mater. Struct. 50 (2017) 253.

[36] T. Ashour, H. Georg, W. Wu, An experimental investigation on equilibrium moisture content of earth plaster with natural reinforcement fibres for straw bale buildings, Appl. Therm. Eng. 31 (2011) 293–303. https://doi.org/https://doi.org/10.1016/j.applthermaleng.2010.09.009.

[37] T. Colinart, P. Glouannec, Temperature dependence of sorption isotherm of hygroscopic building materials. Part 1: Experimental evidence and modeling, Energy Build. 139 (2017) 360–370. https://doi.org/10.1016/j.enbuild.2016.12.082.

[38] ISO 12571:2013(E), International Standard Hygrothermal performance of building materials and products — Determination of hygroscopic sorption properties, 2013.

[39] L. Greenspan, Humidity fixed points of binary saturated aqueous solutions, J. Res. Natl. Bur. Stand. - A. Phys Ics Chem. 81 (1977).

[40] NSAI, EN ISO 12572 - Hygrothermal performance of building materials and products - Determination of water vapour transmission properties, (2001) 1–35.

[41] F. McGregor, A. Fabbri, J. Ferreira, T. Simões, P. Faria, J.-C. Morel, Procedure to determine the impact of the surface film resistance on the hygric properties of composite clay/fibre plasters, Mater. Struct. 50 (2017) 193. https://doi.org/10.1617/s11527-017-1061-3.

[42] H. Janssen, G.A. Scheffler, R. Plagge, Experimental study of dynamic effects in moisture transfer in building materials, Int. J. Heat Mass Transf. 98 (2016) 141–149. https://doi.org/10.1016/j.ijheatmasstransfer.2016.03.031.

[43] O. Vololonirina, B. Perrin, Inquiries into the measurement of vapour permeability of permeable materials, Constr. Build. Mater. 102 (2016) 338–348.

[44] N.A.L. Haffar, Optimization of earth stabilization for building construction applications. Thesis, 2017.

[45] D.M. Nguyen, A.C. Grillet, T.M.H. Diep, Q.B. Bui, M. Woloszyn, Characterization of hygrothermal insulating biomaterials modified by inorganic adsorbents, Heat Mass Transf. Und Stoffuebertragung. 56 (2020) 2473–2485. https://doi.org/10.1007/s00231-020-02873-2.

[46] R.L. Danley, New heat flux DSC measurement technique, Thermochim. Acta. 395 (2002) 201–208. https://doi.org/10.1016/S0040-6031(02)00212-5.

[47] L. Soudani, Modelling and experimental validation of the hygrothermal performances of earth as a building material, Thesis at University of Lyon, 2016. Thesis in Civil Engineerin.

[48] A. Fabbri, L. Soudani, F. Mcgregor, J. Morel, Analysis of the water absorption test to assess the intrinsic permeability of earthen materials, Constr. Build. Mater. 199 (2019) 154–162. https://doi.org/10.1016/j.conbuildmat.2018.12.014.

[49] ANFOR, Perofmance hygrothermique des materiaux et produits pour le batiment NF EN ISO 15148, (2003).

[50] M. Hall, Y. Djerbib, Moisture ingress in rammed earth: Part 1 - The effect of soil particle-size distribution on the rate of capillary suction, Constr. Build. Mater. 18 (2004) 269–280. https://doi.org/10.1016/j.conbuildmat.2003.11.002.

[51] T. Chitimbo, N. Prime, F.A. Samad, O. Plé, Effect of capillary rise on mechanical behaviour of unstabilized rammed earth, in: NoMaD, 2022: pp. 1–6.

[52] M. Thommes, K. Kaneko, A. V. Neimark, J.P. Olivier, F. Rodriguez-Reinoso, J. Rouquerol, K.S.W. Sing, Physisorption of gases, with special reference to the evaluation of surface area and pore size distribution (IUPAC Technical Report), Pure Appl. Chem. 87 (2015) 1051–1069. https://doi.org/10.1515/pac-2014-1117.

[53] L. Zhang, L. Yang, B.P. Jelle, Y. Wang, A. Gustavsen, Hygrothermal properties of compressed earthen bricks, Constr. Build. Mater. 162 (2018) 576–583. https://doi.org/10.1016/j.conbuildmat.2017.11.163.

[54] P. Eizaguirre, A.M. Tang, B. Maillet, R. Sidi-Boulenouar, B. Chabot, M. Bornert, J.M. Pereira, P. Dangla, P. Aimedieu, J. Talandier, M.N. Vu, Impact of sand on the water retention properties of a bentonite/sand mixture by NMR characterization, E3S Web Conf. 382 (2023) 0–5. https://doi.org/10.1051/e3sconf/202338214003.

[55] H. Cagnon, J.E. Aubert, M. Coutand, C. Magniont, Hygrothermal properties of earth bricks, Energy Build. 80 (2014) 208–217. https://doi.org/10.1016/j.enbuild.2014.05.024.

[56] Redige sous Direction Collectif des Associaiton et Federation Terre Crue, Guide des bonnes pratiques de la constuction en terre crue, complet, edition 13 décembre 2018, n.d. https://www.rehabilitation-

bati-ancien.fr/espace-documentaire/guide-des-bonnes-pratiques-la-construction-en-terre-crue [18/04/2022].

[57] D. Medjelekh, L. Ulmet, F. Dubois, Characterization of hygrothermal transfers in the unfired earth, Energy Procedia. 139 (2017) 487–492. https://doi.org/10.1016/j.egypro.2017.11.242.

[58] M. Hall, D. Allinson, Assessing the effects of soil grading on the moisture content-dependent thermal conductivity of stabilised rammed earth materials, Appl. Therm. Eng. 29 (2009) 740–747. https://doi.org/10.1016/j.applthermaleng.2008.03.051.

[59] M.W. Labat, Matthieu, Moisture balance assessment at room scale for four cases based on numerical simulations of heat–air–moisture transfers for a realistic occupancy scenario, J. Build. Perform. Simul. 9 (2016) 487–509. https://doi.org/10.1080/19401493.2015.1107136.

[60] J.-P. Laurent, Contribution à la caractérisation thermique des milieux poreux granulaires: optimisation d'outils de mesure" in-situ" des paramètres thermiques, application à l'étude des propriétés thermiques du matériau terre, Grenoble INPG, 1986.

[61] A. Simpson, The effect of moisture on the thermal property of a reed thatch roof during the UK heating season, Energy Build. 257 (2022) 111777. https://doi.org/10.1016/j.enbuild.2021.111777.

[62] E. Simo, P.D. Dzali Mbeumo, J.C. Mbami Njeuten, Moisture Transfer in Concrete: Numerical Determination of the Capillary Conductivity Coefficient, Slovak J. Civ. Eng. 25 (2017) 10–18. https://doi.org/10.1515/sjce-2017-0002.

[63] J. Tan, J. Liang, L. Wan, B. Jiang, Influence of Non-Constant Hygrothermal Parameters on Heat and Moisture Transfer in Rammed Earth Walls, Buildings. 12 (2022). https://doi.org/10.3390/buildings12081077.

[64] U. Dhakal, U. Berardi, M. Gorgolewski, R. Richman, Hygrothermal performance of hempcrete for Ontario (Canada) buildings, J. Clean. Prod. 142 (2017) 3655–3664. https://doi.org/10.1016/j.jclepro.2016.10.102.

[65] A.E. Losini, Rammed earth stabilization with waste or recycled materials and natural additives : characterizations and simulations, Thesis at Universite Savoie Mont Blanc, Génie Civil et Sciences de l'Habitat, 2021.

[66] CRAterre éditions, ed., Passive strategies used in Southern Portugal vernacular rammed earth buildings and their influence in thermal performance, Constr. Build. Mater. 1 (2019) 1–17. https://doi.org/10.1017/CBO9781107415324.004.